

Enhancing the Anticancer Activity of Photodynamic Therapy with Dual Photosensitizers Incorporated Nanoparticle Design

Submitted to the Graduate School of Natural and Applied Sciences
in partial fulfillment of the requirements for the degree of

Master of Science

in Biomedical Engineering

by

Emel Bakay

ORCID 0000-0002-3042-810X

August, 2021

This is to certify that we have read the thesis **Enhancing the Anticancer Activity of Photodynamic Therapy with Dual Photosensitizers Incorporated Nanoparticle Design** submitted by **Emel Bakay**, and it has been judged to be successful, in scope and in quality, at the defense exam and accepted by our jury as a MASTER'S THESIS.

APPROVED BY:

Advisor: **Dr. Nermin Topalođlu Avşar**
İzmir Kâtip Çelebi University

Co-advisor: **Dr. Didem Sen Karaman**
İzmir Kâtip Çelebi University

Committee Members:

Assoc. Prof. Dr. Ozan Karaman
İzmir Kâtip Çelebi University

Dr. Gizem Kaleli Can
İzmir Democracy University

Date of Defense: August 23, 2021

Declaration of Authorship

I, **Emel Bakay**, declare that this thesis titled **Enhancing the Anticancer Activity of Photodynamic Therapy with Dual Photosensitizers Incorporated Nanoparticle Design** and the work presented in it are my own. I confirm that:

- This work was done wholly or mainly while in candidature for the Master's / Doctoral degree at this university.
- Where any part of this thesis has previously been submitted for a degree or any other qualification at this university or any other institution, this has been clearly stated.
- Where I have consulted the published work of others, this is always clearly attributed.
- Where I have quoted from the work of others, the source is always given. This thesis is entirely my own work, with the exception of such quotations.
- I have acknowledged all major sources of assistance.
- Where the thesis is based on work done by myself jointly with others, I have made clear exactly what was done by others and what I have contributed myself.

Signature:

Date:

10.08.2021

Enhancing the Anticancer Activity of Photodynamic Therapy with Dual Photosensitizers Incorporated Nanoparticle Design

Abstract

Photodynamic Therapy (PDT) is a kind of light therapy for the treatment of important diseases that the world is fighting, such as cancer and infection. After the application of light-sensitive and non-toxic agents to the diseased tissue, light applications provide the death of the diseased cells. Thus, PDT is a therapeutic and curative method. The use of PDT for the treatment of different types of cancer is quite common. It has been the subject of many cancer types of research because it has minimal side effects and it is not possible for the disease to develop resistance as a result of the natural progression of its mechanism. Today, nanoparticle technology is used in many studies examining the anticancer activity of PDT. Different types of nanoparticles are used with different designs for diagnosis and treatment purposes. It increases the effectiveness of PDT in many ways. It provides many advantages such as the successful transfer of photosensitive agents to the diseased tissue and accumulation only in the target cells or preventing their activation before light application. In this study, the effectiveness of PDT was increased on PC3 prostate cancer by the creation of a dual nanoparticle and laser system design. Mesoporous silica nanoparticles (MSN) have been used as a carrier because of their specific physical properties such as biocompatibility or tunability. MSN nanoparticles were formed with Chlorin e6 (Ce6), then indocyanine

green (ICG) was loaded into the pores of MSN. The formed dual photosensitizer incorporated nanoparticles were simultaneously excited with the wavelengths of 655 and 808 nm, and anticancer activity was investigated. Dual photosensitizer incorporated nanoparticles at 25, 50, and 100 $\mu\text{g/ml}$ concentrations were applied to cancer cells. As a result of dual laser application, increased anticancer photodynamic activity was observed with the increasing nanoparticle concentrations. Increased PDT effectiveness has been proven by different analysis methods.

Keywords: Photodynamic Therapy, Chlorin e6, Indocyanine Green, Mesoporous Silica Nanoparticles, PC3 Prostate Cancer Cells

Dual Fotosensitizan İeren Nanoparacık Tasarımı ile Fotodinamik Terapinin Antikanser EtkinliĐinin Geliřtirilmesi

ÖZ

Fotodinamik Terapi (PDT), kanser ve enfeksiyon gibi dünyanın mücadele ettiĐi önemli hastalıkların tedavisine yönelik bir tür ışık tedavisidir. IşıĐa duyarlı ve toksik olmayan ajanların hastalıklı dokuya uygulanmasından sonra hafif uygulamalar hastalıklı hücrelerin ölümünü sağlar. Bu nedenle, PDT tedavi edici ve iyileřtirici bir yöntemdir. Farklı kanser türlerinin tedavisinde PDT kullanımı oldukça yaygındır. Yan etkilerinin minimal olması ve mekanizmasının doğal seyri sonucunda hastalığın diren geliřtirmesi mümkün olmadığı için birçok kanser arařtırmasına konu olmuřtur. Günümüzde nanopartikül teknolojisi, PDT'nin antikanser aktivitesini inceleyen birçok alıřmada kullanılmaktadır. Teřhis ve tedavi amacıyla farklı tasarımlarda farklı tipte nanopartiküller kullanılmaktadır. PDT'nin etkinliĐini birçok yönden artırır. IşıĐa duyarlı ajanların hastalıklı dokuya başarılı bir řekilde aktarılması ve sadece hedef hücrelerde birikmesi veya ışık uygulanmadan önce aktivasyonlarının engellenmesi gibi birçok avantaj sağlar. Bu alıřmada, ikili nanopartikül ve lazer sistem tasarımı oluşturularak PC3 prostat kanserinde PDT'nin etkinliĐi artırılmıřtır. Mezogözenekli silika nanopartiküller (MSN), biyouyumluluk veya ayarlanabilirlik gibi spesifik fiziksel özelliklerinden dolayı taşıyıcı olarak kullanılmıřtır. Klorin e6 (Ce6) ile MSN nanoparacıkları oluşturulmuř, ardından MSN'nin gözeneklerine indosiyanin yeřili

(ICG) yüklenmiştir. Oluşturulan ikili ışığa duyarlılaştırıcı içeren nanopartiküller, 655 ve 808 nm dalga boyları ile eş zamanlı olarak uyarıldı ve antikanser aktivitesi araştırıldı. Kansere hücrelerine 25, 50 ve 100 µg/ml konsantrasyonlarında nanopartiküller içeren ikili ışığa duyarlılaştırıcı uygulandı. Çift lazer uygulaması sonucunda artan nanopartikül konsantrasyonları ile antikanser fotodinamik aktivitenin arttığı gözlemlendi. Artan PDT etkinliği, farklı analiz yöntemleriyle kanıtlanmıştır.

Anahtar Kelimeler: Fotodinamik Terapi, Klorin e6, İndosiyenin Yeşil, Mezogözenekli Silika Nanoparçacıkları, PC3 Prostat Kansere Hücreleri

To my lovely family...

Acknowledgment

This study was supported by the Scientific and Technological Research Council of Turkey (TUBITAK Project No: 219S125).

First of all, I would like to thank my supervisor, Dr. Nermin Topalođlu Avşar, with whom I have worked for years and who contributed to me in every sense. I am grateful to her because she is always a patient, respectful, loving, and friendly attitude to me. Thank you so much for the opportunities she gave me. During this study, I was very pleased to work under his academic supervision.

Secondly, I would like to thank my co-advisor, Dr. Didem Sen Karaman. Thank you very much for always helping in the experiments, for her friendly and loving attitude, for her valuable advice. I am grateful to her for the different perspectives she has given me in this work.

I would like to thank my colics and friends are Dilara Portakal Koç, Hilal Er, Tansu Gölcez, Ziyşan Buse Yaralı Çevik and Ayşenur Pamukçu for their help in the experiments and for sharing my day in the laboratory environment.

And lastly, thanks to my lovely family for always supporting me.

Table of Contents

Declaration of Authorship	ii
Abstract	iii
Öz	iv
Acknowledgment	vi
List of Figures	x
List of Tables.....	xi
List of Abbreviations.....	xii
List of Symbols	xiii
1 Introduction	1
1.1 Photodynamic Therapy	2
1.1.1 Molecular Mechanisms of Photodynamic Therapy.....	3
1.1.2 Light Sources	6
1.1.3 Light Sensitive Agents.....	6
1.1.4 Pros and Cons	7
1.2 Nanoparticles	8
1.2.1 Nanoparticles in Photodynamic Therapy	9
1.2.2 Mesoporous Silica Nanoparticles in Photodynamic Therapy.....	10
1.3 Photodynamic Therapy for Cancer Treatment.....	13
2 Materials and Methods	15
2.1 Cell Culture.....	16
2.2 Preperation of Chlorin e6 and Indocyanine Green Incorporated Mesoporous Silica Nanoparticles	17
2.2.1 Synthesis of MSN with Chlorin e6.....	17

2.2.2	Surface Modification of MSN-Ce6 with Polypropyleneimine.....	18
2.2.3	Indocyanine Green Loading into the Pores of MSN-Ce6@PPI.....	18
2.3	Physico-Chemical Characterizations of the Nanoparticles.....	19
2.4	Light Sources and Dual Optical System	20
2.5	Experimental Groups	21
2.6	In Vitro Analysis.....	22
2.6.1	Cytotoxicity Investigations of the Nanoparticles on PC3 Prostate Cancer and L929 Fibroblast Cells	22
2.6.2	Photo-Toxicity Analysis of the Nanoparticles on PC3 Prostate Cancer and L929 Fibroblast Cells after PDT Applications	23
2.7	Cellular Uptake of Nanoparticles into PC3 Cells	24
2.8	Analysis of the Intracellular ROS Production in PC3 Cells after PDT Applications	24
2.9	Analysis of the Mitochondrial Membrane Potential Change in PC3 Cells after PDT Applications.....	25
2.10	Analysis of the Nitric Oxide Release in PC3 Cells after PDT Applications	25
2.11	Live/Dead Cell Analysis via Acridine Orange/Propidium Iodide Staining of PC3 Cells after PDT Applications	26
2.12	Apoptosis Analysis via DAPI Staining in PC3 Cells.....	26
2.13	Temperature Measurements	27
2.14	Statistical Analysis.....	27
3	Results and Discussion	28
3.1	Preparation of MSN-Ce6@PPI-ICG Nanoparticles	28
3.1.1	Synthesis of MSN-Ce6 Nanoparticles	28
3.1.2	PPI Surface Modification of MSN-Ce6 Nanoparticles	30
3.1.3	ICG Loading to the MSN-Ce6@PPI Nanoparticles.....	32
3.2	Singlet Oxygen Generation Capacity of MSN-Ce6@PPI-ICG Nanoparticles	35
3.3	Viability Analysis	37
3.3.1	MTT Analysis.....	37

3.3.2 Cellular Uptake of MSN-Ce6@PPI-ICG Nanoparticles in PC3 Cells	44
3.3.3 Acridine Orange/Propidium Iodide Staining.....	45
3.3.4 DAPI Staining.....	46
3.4 Mechanistic Analysis	48
3.4.1 Reactive Oxygen Species Measurements in PC3 Cells after the PDT Applications.....	48
3.4.2 Mitochondrial Membrane Potential of PC3 Cells after PDT Applications.....	50
3.4.3 Nitric Oxide Releasing in PC3 Cells after the PDT Applications....	52
3.5 Temperature Measurements during Dual Laser Optical System Applications	53
4 Conclusion.....	56
References	58
Curriculum Vitae	69

List of Figures

Figure 1.1 Photodynamic Therapy Application Procedure	3
Figure 1.1.1 Molecular Mechanisms of Photodynamic Therapy	5
Figure 1.2 Usage Areas of Nanomaterial Technology	9
Figure 2 The progress of the study, the methods and, their characterizations.....	16
Figure 2.4 Dual Laser Optical System.....	21
Figure 3.1.1a) SEM image of MSN nanoparticles produced with Ce6 photosensitizer. b) Size distribution, average hydrodynamic diameter, PDI value and Zeta potential data of 0.2 mg/mL Ce6-MSN prepared in HEPES buffer solution (pH 7.2, 25 mM).....	29
Figure 3.1.1a a) Absorbance Spectrum of 2.5 $\mu\text{g/mL}$ Ce6 and ICG photosensitizer b) The absorbance values corresponding to the increasing concentrations of Ce6 and ICG photosensitizers and the obtained calibration curves, Inset figure; absorbance spectrum of the combined solution of free 2.5 $\mu\text{g/mL}$ Ce6 and ICG photosensitizers.....	30
Figure 3.1.3 Absorbance spectrum of 0.1 mg/mL Ce6-MSN@PPI-ICG(20) in DMSO and the initial loading amount of ICG is 20%.....	35
Figure 3.2 a) Singlet oxygen ratio of Ce6-MSN@PPI-ICG(5%) at different concentrations before and after stimulation with dual laser optic system b) singlet oxygen ratio of free photosensitizers before and after stimulation with dual laser optic system (for 10 $\mu\text{g/mL}$ nanoparticle: 0.24 $\mu\text{g/mL}$ Ce6 and 0.045 $\mu\text{g/mL}$ ICG, for 100 $\mu\text{g/mL}$ nanoparticle: 2.4 $\mu\text{g/mL}$ Ce6 and 1.8 $\mu\text{g/mL}$ ICG, for 200 $\mu\text{g/mL}$ nanoparticle: 4.8 $\mu\text{g/mL}$ Ce6 and 3.6 $\mu\text{g/mL}$ ICG, for 400 $\mu\text{g/mL}$ nanoparticle: 9.16 $\mu\text{g/mL}$ Ce6 and 7.2 $\mu\text{g/mL}$ ICG) c) 25, 50, and 100 $\mu\text{g/mL}$ nanoparticle DPBF spectrum of Ce6- MSN@PPI-ICG(%5) nanoparticles before and after dual laser optic	

system. The samples were carried out for DBPF analysis in DMSO and the initial loading amount of ICG is 5%	36
Figure 3.3.1a Cell viability of 1, 5, 10, 25, 50, 100, 400 $\mu\text{g}/\text{mL}$ MSN-Ce6@PPI-ICG (%5) nanoparticles after the 4h and 24h incubation time on PC3 cells. Statistically significant results are represented with * ($P < 0.05$)	38
Figure 3.3.1b Cell viability of 25, 50, and 100 $\mu\text{g}/\text{mL}$ MSN-Ce6@PPI-ICG (%5) nanoparticles at immediately after applications and 24h after the applications on L929 cells. Statistically significant results are represented with * ($P < 0.05$)	39
Figure 3.3.1c Cell viability of only dual laser light, 5, 10, 25, 50, and 100 $\mu\text{g}/\text{mL}$ MSN-Ce6@PPI-ICG (%5) nanoparticles with dual-laser application after the 4h and 24h incubation time on PC3 cells. Statistically significant results are represented with * ($P < 0.05$)	40
Figure 3.3.1d Cell viability of only dual laser, 25, 50, and 100 $\mu\text{g}/\text{mL}$ MSN-Ce6@PPI-ICG (%5) nanoparticles with dual laser light at immediately after applications and 24h after the applications on L929 cells. Statistically significant results are represented with * ($P < 0.05$)	42
Figure 3.3.1e Cell viability with free Ce6 and ICG photosensitizers that are found inside of the 25, 50 and 100 $\mu\text{g}/\text{mL}$ MSN-Ce6@PPI-ICG nanoparticles and their PDT applications with dual laser light on PC3 cells (Free photosensitizer concentrations; for 25 $\mu\text{g}/\text{mL}$ nanoparticle: 0.6 $\mu\text{g}/\text{mL}$ Ce6 and 0.45 $\mu\text{g}/\text{mL}$ ICG, for 50 $\mu\text{g}/\text{mL}$ nanoparticle: 1.2 $\mu\text{g}/\text{mL}$ Ce6 and 0.9 $\mu\text{g}/\text{mL}$ ICG, for 100 $\mu\text{g}/\text{mL}$ nanoparticle: 2.4 $\mu\text{g}/\text{mL}$ Ce6 and 1.8 $\mu\text{g}/\text{mL}$ ICG and dual laser parameters; for 655nm diode laser; 300mW power, 120J/cm ² energy density, for 808nm diode laser; 600mW power, 240J/cm ² energy density, 706s application time). Statistically significant results are represented with * ($P < 0.05$)	44
Figure 3.3.2 Absorbance Spektrum of 25, 50 and 100 $\mu\text{g}/\text{mL}$ MSN-Ce6@PPI-ICG nanoparticles in Triton-100X and PC3 cell solutions after 24h incubation.	45
Figure 3.3.3 Acridine orange (live cell, green) / Propidium Iodide (dead cell, red) images of dual laser, 25, 50 and 100 $\mu\text{g}/\text{mL}$ MSN-Ce6@PPI-ICG	

nanoparticles and their PDT applications with dual laser application on PC-3 cells.	46
Figure 3.3.4 DAPI Staining images of PDT groups with 25, 50 and 100 $\mu\text{g}/\text{mL}$ MSN-Ce6@PPI-ICG nanoparticles and dual optic laser light application on PC-3 cells.	47
Figure 3.4.1 Reactive Oxygen Species formation of dual laser light, 25, 50, and 100 $\mu\text{g}/\text{mL}$ nanoparticles and their PDT groups with dual laser on PC3 cells. Statistically significant results are represented with * ($P < 0.05$)	49
Figure 3.4.2 JC-1 Mitochondrial Membrane Potential Assay Measurements a) Flouresence values of dual laser light, 25, 50 and 100 $\mu\text{g}/\text{mL}$ MSN-Ce6@PPI-ICG nanoparticles and their PDT applications on PC3 cells b) JC-1 Aggregates images of living cells in dual laser light, 25, 50 and 100 $\mu\text{g}/\text{mL}$ MSN-Ce6@PPI-ICG nanoparticles and their PDT applications on PC3 cells. Statistically significant results are represented with * ($P < 0.05$).	51
Figure 3.4.3 Nitrite amounts of dual laser light, 25, 50 and 100 $\mu\text{g}/\text{mL}$ MSN-Ce6@PPI-ICG nanoparticles and their PDT applications with dual laser on PC-3 cells. Statistically significant results are represented with * ($P < 0.05$).....	53
Figure 3.5 Temperature Measurements with thermal camera for dual laser light, PDT25, PDT50, and PDT100 groups.....	55

List of Tables

Table 3.1.2 Zeta Potential and DLS results before and after surface modification ...	31
Table 3.1.3a Zeta Potential and DLS results of MSN-Ce6@PPI-ICG nanoparticles with different loading rates	33
Table 3.1.3b Amount of ICG loaded on MSN-Ce6 and MSN-Ce6@PPI nanoparticles	34

List of Abbreviations

APTES	3-Aminopropiltrietsoksisilan
Ce6	Chlorin e6
CFU	Colony Forming Unit
CTAB	Cetyltrimethylammonium Bromide
Cur	Curcimin
DAPI	4',6-diamidino-2-phenylindole
DCF	Dichlorofluorescin
DCFHA-DA	2', 7'- dichlorofluorescin Diacetate
DCM	Dichloromethane
DLS	Dynamic Light Scattring
DMEM	Dulbecco's Modified Eagle's Medium
DMSO	Dimethylsulfoxide
DNA	Deoxyribonucleic Acid
DOX	Doxorubicin
EDC	1-ethyl-3-(3-dimethylaminoprophyl)carbodiimide
EDTA	Ethylenediaminetetraacetate
EPR	Enhanced Permeation and Retention
FBS	Fetal Bovine Serum
ICG	Indocyanine Green
L929	Fibroblast Cell Line
LED	Light Emitting Diode
MB	Methylene Blue

MMP	Mitochondrial Membrane Potential
MSN	Mesoporous Silica Nanoparticle
MTT	(3-(4,5-Dimethylthiazol-2-yl)-2,5-Diphenyltetrazolium Bromide)
NIR	Near Infrared
NO	Nitric Oxide
NP	Nanoparticle
PBS	Phosphate Buffered Saline
PC3	Prostate Cancer Cell Line
PDI	Polydispersity Index
PDT	Photodynamic Therapy
PEG	Polyethylene Glycol
PPI	Polypropylene imine
PS	Photosensitizer
RB	Rose Bengal
ROS	Reactive Oxygen Species
RPMI	Roswell Park Memorial Institute
SEM	Scanning Electron Microscopy
TBO	Toluidine Blue Ortho
TEOS	Tetraethyl Orthosilicate
UCNP	Upconversion Nanoparticle

List of Symbols

L	Liter
μ	Micro
$^{\circ}C$	Celcius
S^0	Singlet State
S^1	Excited Singlet State
T^1	Excited Triplet State

Chapter 1

Introduction

Cancer has been known for many years as a challenging disease that is difficult to treat and seriously threatens human life. With the development of technology and treatment methods, it has now become possible to treat many cancer types under certain conditions. However, treatment methods such as chemotherapy, radiotherapy, or surgical methods with known effectiveness cause very serious side effects on patients. Side effects may cause different complications after the treatment and they may cause serious risks on the patient's life. The aggressiveness of the disease after surgical operations, the increase in the rate of spread, or the occurrence of various infections can be given as examples. For this reason, innovative treatment methods are being developed in addition to traditional treatment methods for the treatment of cancer. Photodynamic Therapy (PDT) is a candidate to be used in this sense and is a treatment method that has minimal side effects. It causes tissue damage on cancerous tissue by using light-sensitive non-toxic agents together with light. In addition, because its effective mechanism works with natural processes, it does not show serious side effects and resistance development. PDT application on prostate cancer, which is the most prevalent type of cancer among male patients due to the side effects of traditional treatment methods, is very promising. In addition, the use of nanotechnology during the delivery of photosensitive agents to cancerous tissue has become very popular in PDT recently. Thus, the maximum anti-cancer effect can be observed with the application of light and photosensitive agents at minimum doses.

1.1 Photodynamic Therapy

The concept of photodynamic therapy (PDT) originated in 1900 by the coincidence of German medical student Oscar Raab and his supervisor Prof. Hermann von Tappeiner. Oscar Raab and von Tappeiner noticed that a type of aquatic paramecia died when exposed to sunlight through the window during incubation with acridine orange [1]. Later, von Tappeiner and Jesionek, a dermatologist in Munich, stained and illuminated the cells with xanthene dye eosin on a patient with basal cell carcinoma. This investigation is the first use of PDT in the treatment of a disease and its discovery as a treatment method [2]. Based on the first experienced applications, PDT can be defined as the healing of the diseased tissue with the light application after the light-sensitive dyes penetrate the diseased tissue. Later on, the studies have progressed in the field of improving the efficacy of PDT on animal models and the discovery of different photosensitive dyes. The researches so far have highlighted PDT as a potential therapeutic approach in the treatment of malignant and infectious diseases caused by microorganisms and will continue to increase the use of PDT in the future [3].

In PDT, the photosensitive agents should be correctly delivered to the diseased area of the body with different delivery methods [4]. In this region, the diseased cells are allowed to uptake the light-sensitive substance for a certain period (incubation time). After the cellular uptake of light-sensitive agents, the excess of light-sensitive agents in the environment is removed to provide a selective treatment. After the light is applied via superficial or interstitial methods to the target area, healing occurs as a result of damage on diseased cells [4, 5]. As a molecular mechanism, it is complex and many molecules participate in it that result in apoptosis/necrosis.

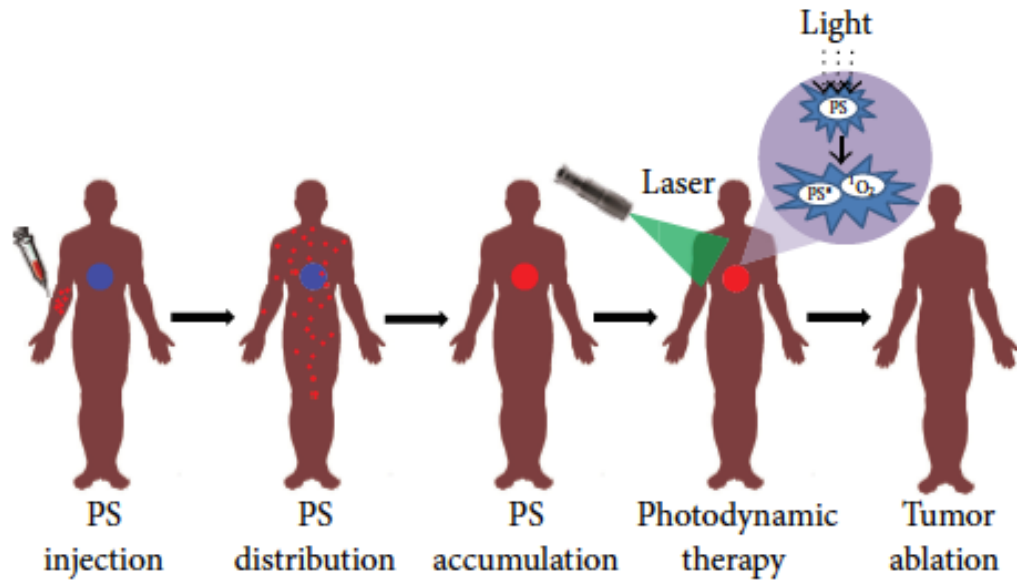


Figure 1.1: Photodynamic Therapy Application Procedure [6]

1.1.1 Molecular Mechanisms of Photodynamic Therapy

PDT is a treatment method that creates biological effects as a result of photophysical and photochemical processes. PDT has a working mechanism that includes photosensitive dyes called photosensitizer (PS), light, and molecular oxygen that do not cause any toxic effects alone but cause phototoxicity when they are present together. Photosensitizers can induce certain reactions by absorbing specific wavelengths depending on their molecular structure and transferring this energy to the surrounding molecules [7, 8]. It causes selective damage and cell death on cancer cells or microorganisms as a result of the non-thermal photochemical reactions performed by the PS atoms after which are activated as a result of light application [8]. Oxygenated harmful products (Reactive oxygen species, ROS) formed as a result of these photochemical reactions play an important role in the cell death mechanism. The pathways and reaction types of the photodynamic therapy may vary, depending on the amount and location of molecular oxygen, the wavelength of the applied light and the molecular structure of PS [7, 8, 9].

The photodynamic process begins with the absorption of light by the atoms of PS. PS atoms that are found at the ground state absorb the light energy and jump to the highly energetic excited state. This level is called the singlet excited state and is the short-

lived level for PS atoms. These excited atoms want to return to their stable forms at the ground state. For this reason, PS atoms return to the ground state by emitting light (fluorescence) or with internal conversion and they release their energy. These conditions are not among the reactions that play a role in the PDT mechanism but fluorescence can use fluorescence imaging or measure the pharmacokinetics and distribution of the PS [10]. PS atoms found in singlet excited state, besides the mentioned photophysical events mentioned before, can go into a process called intersystem crossing. In the intersystem crossing process, PS atoms in the singlet excited state can switch to the level called the triplet excited state, and they cannot easily return to the ground state due to the parallel spins of excited electrons at this level (spin-forbidden process). For this reason, the duration of PS atoms is long-lived according to the singlet excited state. But even triplet excited PS atom can return the ground state and it can emit light (phosphorescence). Triplet excited state PS atoms may react with the biological substrate and oxygen, partly because they stay longer at that excited state, creating oxidative damage, which is the natural damage mechanism of PDT [10, 11, 12]. In the PDT mechanism, the reactive oxygen species (ROS) that cause the photodynamic effect takes place through two different photochemical reaction pathways called Type I Reactions and Type II Reactions (13).

In the Type, I mechanism, oxygen or hydrogen transfer occurs between triplet excited state PS atoms and cellular substrates. As a result, radical anions or cations can be formed directly or indirectly. Electron transfer with molecular oxygen creates a superoxide anion, which is not toxic alone for biological systems. Superoxide anion plays a role in different reactions involving hydrogen peroxide and oxygen formation. Hydrogen peroxide plays an important role in the formation of hydroxyl radical, which has biological toxicity. Hydroxyl radicals can easily pass through cell membranes and create cellular damage with diffusion logic. In other words, it can bind to organic substrates such as fatty acids or lipids and oxidize them and the resulting products become reactive. All these reactive products can react with different substrates so that cellular destruction can continue in a cascade of reactions. Since hydrogen peroxide, like hydroxyl radical, can easily pass through cell membranes, both radicals also can damage the organelles in the cytoplasm of the cells. Also, highly reactive hydroperoxyl radicals can be formed by the reaction of superoxide with nitric oxide, which is also a radical [10, 13, 14]. The Type I mechanism usually takes place in the presence of a

low concentration of molecular oxygen. Increasing oxygen concentration to high levels can trigger Type II mechanisms as well as Type I mechanisms [9].

Type II mechanisms are more likely to occur in biological structures with high oxygen concentrations [9]. Often organic substrate molecules are found in the singlet ground state, whereas oxygen is present in the triplet ground state. For this reason, energy transfer occurs easily between excited triplet state PS atoms and ground triplet state oxygen atoms (spin-allowed). As a result of this energy transfer, reactive singlet oxygen radicals are produced [10, 15]. The reactive singlet oxygen attacks the cellular components of microbial and malignant cells such as nucleic acid, lipid, or protein, causing irreversible cellular destruction. These cellular inactivations and destructions are spatially limited and selectively occur in the environment in which it occurs [16]. These two mechanisms can proceed simultaneously in the biological structure. Which type of reaction is dominant and lethal depends on many properties such as PS structure, the oxygen concentration of the environment, amount of substrate, tissue dielectric constant, or pH. These features also affect the success of PDT [8, 10, 16].

Creating an ideal PDT mechanism and an effective photodynamic effect does not depend only on these properties. The light sources and PSs that are used need to be examined separately.

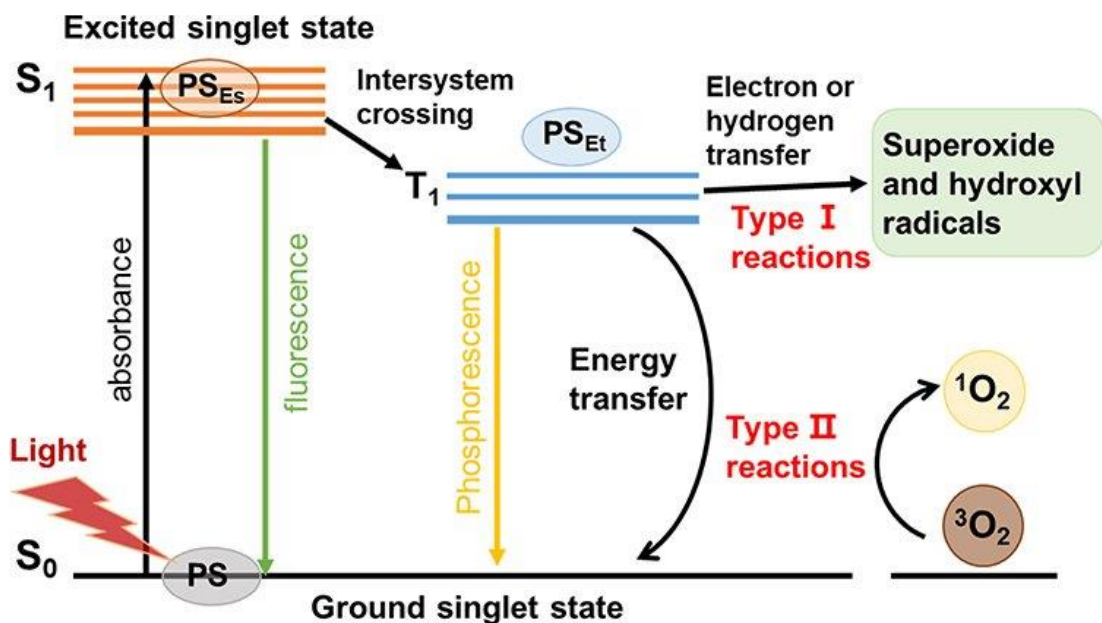


Figure 1.1.1: Molecular Mechanisms of Photodynamic Therapy [17]

1.1.2 Light Sources

In PDT applications, the properties of light vary according to the location of the target tissue in the body and the absorption band of the PS used [18]. Optimizing the wavelength, energy density, and power of the light used is necessary for an effective PDT mechanism. The wavelength range of 600-850 nm is preferred in these types of light therapies and it is called the therapeutic window. Because wavelengths in this range have the photon energy that can stimulate PS atoms [7, 19]. Besides, the longer wavelengths can penetrate the tissue easily and deeply. For this reason, light sources with longer wavelengths are preferred in PDT applications for deeper treatments [20]. Laser devices, LEDs, lamps, and daylight can be used as light sources in PDT applications [21, 22]. However, it has been shown by different studies that laser light provides an advantage over other light sources and creates a more effective photodynamic effect because of its unique properties such as being monochromatic and coherent [22, 23]. Specific apparatus for surface illumination or optical fibers can be used to transmit light to the target area to be applied [15].

1.1.3 Light Sensitive Agents

In a basic sense, PS is called the chemical substance that allows light transfer in its environment. Many natural or synthetic PS agents have been produced for PDT, such as chlorophyll derivatives from plants or bacteria, or synthetic dyes and porphyrins [24]. PSs are divided into 3 classes according to their temporal development. First-generation PSs (hematoporphyrin derivatives), second-generation PSs (porphyrinoid derivatives, 5-aminolevulinic acid, chlorins, phthalocyanines, etc.), and the last class are third-generation PS (combination with targets or surface markers of available PSs) were developed. Different types and structures of PS have been developed such as chlorin e6 (Ce6), indocyanine green (ICG), methylene blue (MB), toluidine blue ortho (TBO) due to the previous generation's deficiencies such as instability, insolubility in water, or inability to provide selectivity [9, 16, 25]. Creating an ideal PS is a field that has acquired a wide range of study today. Most researchers are working on different methods to create excellent properties such as low dark toxicity, high chemical stability, and high quantum yield of singlet oxygen, water-solubility, high

photochemical reactivity, proper different administration, or preferential uptake by target tissue [25, 26].

1.1.4 Pros and Cons

Photodynamic therapy is a very advantageous technique for the treatment of cancer and infection with minimal side effects. Nevertheless, it has still some drawbacks that need to be improved. For example, the location of PS in the cell and its role in photodynamic activity cannot be ignored. Having the ROS level in the cells up to a certain level is a condition that activates the cell survival mechanism and promotes cell proliferation. But if the ROS level exceeds a certain level, it can disrupt the oxidative balance in the cell and cause cell death [27]. The diseased cells are highly sensitive to ROS production due to abnormal metabolic activity [28]. Therefore, ROS-mediated therapeutic approaches can damage the diseased cells more effectively than the healthy cells. In addition, the fact that oxygen is an indispensable element for most biological systems and PDT has an oxygen-dependent mechanism so it is a treatment that cannot develop resistance by diseased cells such as cancer cells or bacterial cells [29]. One of the biggest advantages of the PDT operating mechanism is that it can be localized in a specific region. The high metabolic activity, thus the oxygen concentration in the diseased tissue, and the selective accumulation of PS in the diseased tissue ensure that PDT causes minimal damage to the healthy tissue [10, 16, 28, 30]. In addition, in the PDT mechanism, depending on the intracellular localization of PS, multiple death pathways can be triggered. The localization of PS in the cell determines the localization of ROS. For example, ROS formed in the cell membrane can result in cell membrane destruction and cell integrity disruption, resulting in cell necrosis. ROS damage to the mitochondria may result in apoptosis, and ROS damage created in the lysosome and endoplasmic reticulum may result in autophagy [8, 31]. In the diseased cells, even a small amount of all these damages alone or together may be sufficient for cell death. Researchers have proved with different chemical methods and gene analysis which type of cell led to death [32]. This shows that PDT has a very strong working mechanism. In addition, since most PS is not stored in the nucleus, the possibility of DNA damage is low, which may give an idea that no mutations or cancers will occur in the healthy cells [16]. These situations are perfectly acceptable for PDT

applications. However, like any treatment mechanism, some points need improvement in PDT. This also offers researchers a working window.

Two issues need improvement in the PDT mechanism; the effect of light decreases as it reaches the deeper tissues and the location of PS in the desired tissue. Longer wavelength laser light is preferred to preserve the effectiveness of the light in deeper tissues. The penetration capacity of longer wavelength laser light is higher [33]. In addition, this situation is tried to be improved with the developed fiber optic systems and endoscopic methods [34]. Studies are carried out on the localization of PS in the desired tissue and increase its selection and selectivity [35, 36]. Developing the structures of available PSs by pharmacological means, using them as combinations with different chemicals, adding specific target molecules to the target tissue, or creating PS-nanoparticle structures by nanotechnological methods are widely used methods [36]. Concerning the current study, adding PS to nanoparticles with different physical and chemical methods or using them with nanoparticles increases the efficiency of PS considerably.

1.2 Nanoparticles

Organic or inorganic nano-engineered structures with a size range of 1-1000 nm are called nanoparticles. Nanoparticles are very convenient to use due to their positive aspects such as particle size, shape, porosity, and monodispersibility features that can be easily controlled [37]. Nanoparticles are used in many different fields such as agriculture, industry, technology, engineering, pharmacy, and medicine. Due to their superior features, they can be integrated into any area. It can be used for many purposes such as diagnosis, treatment, imaging, drug release, and drug transport in medicine and pharmacy.

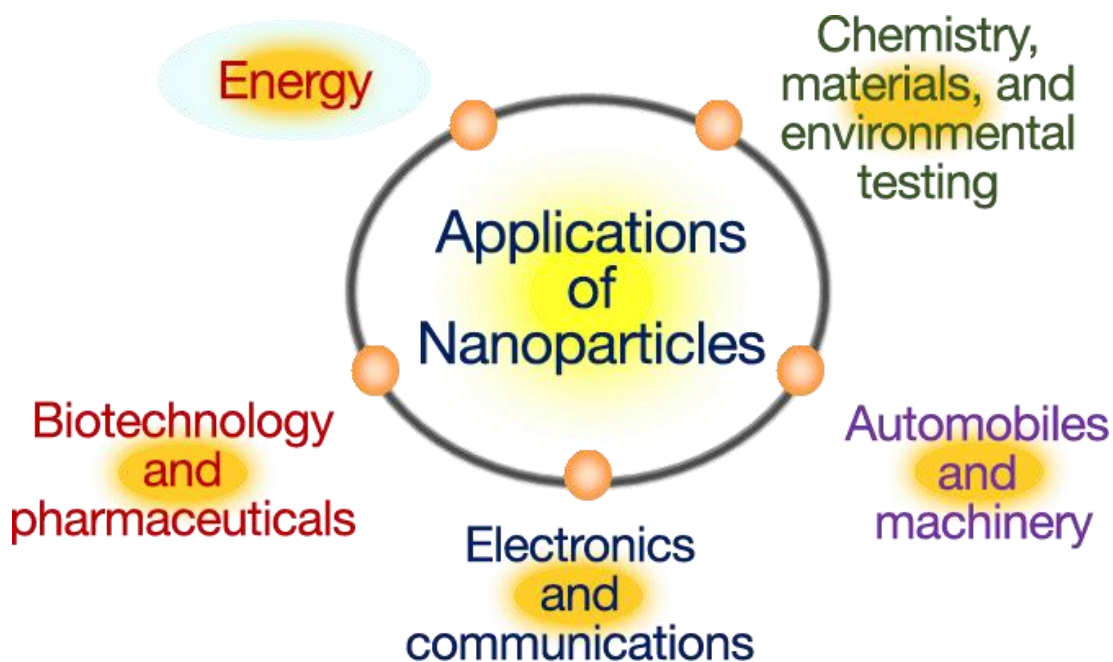


Figure 1.2: Usage Areas of Nanomaterial Technology [38]

1.2.1 Nanoparticles in Photodynamic Therapy

The use of nanotechnology to increase the effectiveness of drugs used for treatment and diagnosis purposes in medicine is a very promising field. The important agents of nanotechnology that can be used in PDT are the nanoparticles that have been created for different purposes. The advantages of using nanoparticles in PDT are numerous; to create enhanced permeability and retention (EPR) effect, the transporting of hydrophobic PSs to the target tissue without degradation, increasing the selectivity, increasing the ROS-forming capacity, improving the water solubility of less soluble PSs, reducing undesirable side effects, etc. [39]. PS can be added to the structure of the nanoparticles in covalent and non-covalent ways during or after synthesis. In covalent bonding, the PS-nanoparticle structure is formed by the way of chemical bonding. Liposomes, dendrimers, or solid nanoparticles are PS-conjugated nanoparticle structures that are examples of covalent bonding. In the non-covalent addition method, the most commonly used strategies are encapsulation and incorporation. Liposomes, micelles, gold nanoparticles, polymer nanoparticles, ceramic nanoparticles, or carbon nanotubes are examples of this type of bonding nanoparticle structure [40, 41]. In addition to these, the use of new generation upconversion nanoparticles (UCNP) in PDT, which is considered to be very new

technology, is expanding. UCNP can convert the energy coming from the photon. In other words, it absorbs the incoming light during light application and emits another radiation with higher energy than the incoming light has. In addition, it increases PDT efficiency in deeper tissues since it absorbs longer wavelengths and emits more energetic light [42]. It increases the selectivity with different target elements or can be combined with different treatment methods as well as PDT with the addition of drugs [43]. The nanoparticles used can be of organic or inorganic origin. Organic structures such as liposomes and polymeric micelles have a high carrying capacity and predictably biocompatible structure in hydrophobic PSs. This means that organic nanostructures alone do not cause any toxicity to biological structures, as predicted. But it only has a limited variety with lipids and some polymers. For this reason, the use of inorganic structures in nanoparticle production has become widespread [44]. Silica, polystyrene, ceramic, magnetic, gold, silver, carbon nanotubes are examples of inorganic nanomaterials. Mesoporous silica nanoparticles are widely used nanoparticles among inorganic nanoparticles. It is very advantageous in terms of its easily adjustable size, biocompatibility, porous structure, and large surface area. Due to its large surface area, it easily allows various functional groups to be incorporated into the nanoparticle structure. Thus, they can be functionalized with different agents.

1.2.2 Mesoporous Silica Nanoparticles in Photodynamic Therapy

Silica is an inorganic material and its main components are sand and glass. It is preferred in nanoparticle production, as it is very suitable to be configured with different functional groups [45]. On the other hand, it allows many PSs to be incorporated into its structure by the physical and chemical methods mentioned above [40, 41]. It is very advantageous to be biocompatible with biological structures [46]. Unlike other nanoparticles, there is no deterioration in its structure due to pH change. The structure, size, and shape of the pores can be easily controlled [47, 48]. PS added to its structure prevents easy release and its porous structure is molecularly permeable. This indicates that the desired PS's photocatalysis capability will be preserved [49]. In addition, being transparent and not absorbing any radiation do not influence the structure and characteristics of the light that is used [50]. For these benefits, quite novel

silica nanoparticles have been developed in anticancer and antibacterial PDT researches.

Even the presence of MSNs in the same environment without chemical or physical bonding with the PS has been shown to increase the effectiveness of PDT [51]. Based on this idea, it is thought that using MSN-PS interaction in PDT can create quite different advantages. Then, it has been reported that the capacity of silica nanoparticles to carry different dyes is favorable. They showed that for the PDT mechanism, the photophysical properties of the dyes do not change and there are different dye loading methods [52]. In the comparative study of Amin and Kaduskar, they formed a system by adsorbing toluidine blue ortho and methylene blue separately to mesoporous silica nanoparticles. They performed antibacterial photodynamic applications on *E. coli*, *P. aeruginosa*, and *S. aureus* bacteria with these MSN-PS systems upon irradiation with 620 nm red light, and they succeeded in the inhibition of the growth of each bacterial strain with different application parameters [53]. Parasuraman et al. investigated the effect of planktonic antimicrobial and antibiofilm in their biofilm forms on two different bacterial strains by encapsulating toluidine blue ortho photosensitizer into mesoporous silica nanoparticles. When TB-MSN was stimulated with a 670 nm red diode laser, they showed a decrease of 5.03 and 5.56 log in CFU/mL of planktonic *P. aeruginosa* and *S. aureus*, respectively. In addition, in their biofilm forms, they provided 66.39% and 76.22% inhibition of biofilm formation, respectively. The antimicrobial and antibiofilm effects of TB alone on each strain and biofilms were almost doubled with the use of MSN [54]. Sun et al. produced composite membranes with the electrospinning method by charging mesoporous silica nanoparticles with methylene blue. They achieved a strong antimicrobial photodynamic effect (<3%) with 660 nm red light application on gram-positive and gram-negative bacterial strains. This idea shows that MSNs and PDT applications are also available in different areas such as packaging besides medicine purposes [55]. Mirzahosseini-pour et al. showed a wound-healing effect in healthy cells with the scratch assay. Results showed as well as a decrease in bacterial cell viability with 465 nm light in planktonic gram-positive *S. aureus*, gram-negative *P. aeruginosa* and their biofilm forms on curcumin-loaded silica nanoparticles [56]. The success of MSN-PDT applications not only on bacteria but also in destroying fungal pathogens is presented as in vitro studies. Parasuraman et al. conducted an antimicrobial photodynamic therapy with MSN and rose bengal

(RB) conjugated functional nanoparticle structure and green light with very low power of 50 mW on *Candida albicans* strains, which can be a source of infection. They achieved 88% and 80% reduction rates on planktonic and biofilm, respectively. This study has presented that the MSN-RB-PDT strategy has a high potential in the use of fungal infections as a treatment method or the sterilization of fungal pathogens [57].

Besides its use in antibacterial PDT, mesoporous silica nanoparticles are more common in the treatment of different localized tumors. The role of MSNs in the use of PDT for anticancer purposes is much more important. Because, as mentioned in detail above, selective accumulation of PS in cancerous tissue or delivery of PS is one of the important points to be improved in PDT. Recent studies have shown that the use of MSN for these purposes changes the results positively [58]. Kuang et al. loaded curcumin, which has low bioavailability, to PEGylated MSNs. With MSN PEGylation, they ensured the escape of nanoparticles from phagocytosis and developed the low-bioavailability and poor solubility problem of curcumin with MSNs. Enhanced anticancer PDT was obtained in PDT groups using MSN-PEG @ Cur compared to PDT groups treated with curcumin-mediated 430 nm light application alone [59]. In another study, MSN nanoparticles were loaded with Ce6 for photodynamic effect and DOX for chemotherapeutic effect. They also provided specific targeting to cancerous cells with hyaluronic acid conjugation. They observed an increasing decrease in the cell viability with increasing nanoparticle concentration on squamous cell carcinoma cells with 670 nm light application [60]. In a similar study combining chemotherapy and PDT on the same platform, cisplatin-resistant lung cancer cells were destroyed by loading Ce6 and cisplatin to MSNs. This study showed that cancer cells that develop resistance to different therapy methods can break the resistance mechanism with the help of PDT [61]. Han et al. reported the use of MSNs with different nanoparticles as well as PS loading. Two MSNs shells were created on the upconversion nanoparticles, the first MSN shell containing methylene blue and the second MSN containing rose bengal. The UCNP has been shown to emit two wavelengths; 660 nm red light for methylene blue excitation and 540 nm green light for rose bengal excitation as a result of the application of 808 nm NIR laser light. DOX drug was conjugated to the pores of this structure containing dual PS for chemotherapy and cyclodextrin to the surface. Thus, DOX drug release could occur as a gatekeeper in the acidic environment of the cancer cell. According to the results of in vitro and in vivo studies, it was understood

that chemo/PDT application is more advantageous than PDT alone or chemotherapy alone [62]. For specific targeting to specific cancer tissue, MSN nanoparticles were coated with membranes obtained from the cancer tissues after photosensitizing loading. This application, which is quite new and specific, showed more effective results as a result of irradiation compared to groups without membranes [63]. In addition, like advanced technology, by adding photosensitizers and carbon dot or radiolabel agents to MSNs, imaging and treatment purposes are provided at the same time in cancer treatment. It has been shown in the studies that the structure of the MSN is suitable for the different methods mentioned [64, 65]. There are also anticancer PDT studies with MSNs on prostate cancer, which is the focus of the current study.

1.3 Photodynamic Therapy for Cancer Treatment

Cancer occurs when abnormal cells in the body divide and multiply uncontrollably. Cancerous cells can spread to different parts of the body by transport and cause cancer metastasis. Cancer can occur in many tissues of the human body. Many people in the world who are fighting against different types of cancer lose their lives. Prostate cancer has recently been the second most common type of cancer in men worldwide. Although many cases and deaths were detected in 2020, the risk of having prostate cancer in a man's life was announced as 11.6% [66]. There may be a certain survival period in localized prostate cancer, whereas in advanced prostate cancer, that is, prostate cancer that recurrence after a certain treatment is fatal [67]. Surgical application, chemotherapy, and radiation therapy are generally quite common, like any other type of cancer. Although these methods are successful, side effects that reduce the quality of life such as urinary symptoms and sexual dysfunctions may occur in patients after the procedures [68]. For these reasons, the use of PDT in the treatment of prostate cancer is very old. The first use of PDT in urology was in 1975 with the application of hematoporphyrin on human bladder carcinoma by Kell et al. [69]. Later, PDT applications with porphyrin derivatives have increased in this area and strategies have been developed that target not only tumor cells but also the vessels that provide blood transmission to them [70, 71]. Looking at current studies, we can see studies in which PDT is supported alone or with MSNs-mediated agents. In a study conducted on human colorectal cancer, effective results of PDT applied with 5-aminolevic acid were reported [72]. They obtained effective photodynamic results at doses of 300

$\mu\text{g/ml}$ and $1\text{-}5\text{ mg/ml}$, respectively, on colon carcinoma and the prostate bacterium *E. coli* of the structure formed by encapsulating protoporphyrin IX into mesoporous organo-silicas [73]. Bouffard et al. associated MSNs with targeting biomarkers, reducing the incubation time, and increasing cell death [74]. With the development of new PSs and the creation of 3rd generation PSs, trials have been made on the prostate [75, 76]. Particle size, pore structure, shape, and content of the nanoparticle used are very important for cytotoxicity and PDT application [77].

This study, it was aimed to create phototoxicity on prostate cancer cells by improving the efficacy of PDT with dual photosensitizer incorporated nanoparticle design and dual laser application. For this, Ce6 and ICG photosensitizers were loaded into MSN nanoparticles. Taking advantage of the positive properties of photosensitizers, the negative properties were eliminated with the nanoparticle design. The concentrations of photosensitizers used with the nanoparticle design were reduced to minimum levels and increased the uptake of photosensitizers into the cancer cells. In addition, a dual laser system has been installed that will enable 655 nm and 808 nm laser devices to be focused on the same point. By simultaneous excitation of the nanoparticle system with 655 nm and 808 nm of wavelengths, the PDT efficiency was increased. In addition, loading the dual photosensitizers into the same nanoparticle also reduced the nanoparticle concentration and light dosage. Thus, maximum PDT efficiency was achieved with a dual nanoparticle and dual laser system. The viability, ROS analysis, mitochondrial membrane potential analysis, nitric oxide analysis, cellular uptake, acridine orange/propidium iodide, and DAPI results showed that this study is very useful and promising for in vivo or clinical research.

Chapter 2

Materials and Methods

This study had three main steps in general. The applications are described below as a summary in Figure 2. To improve photodynamic therapy and increase its anticancer activity, firstly, the creation of a dual structure photosensitizer was carried out. The production of dual-structured nanoparticles includes three steps in itself. In the first stage, Ce6 loaded mesoporous silica nanoparticles (MSN-Ce6) were produced by adding Ce6 photosensitizer to the mesoporous silica matrix. After morphological, size/surface charge analysis, and spectroscopic analyzes were performed on nanoparticles, Ce6 loading amount was determined. Afterward, the surface was coated with hyper-branched cationic polypropyleneimine polymer (PPI) to increase the amount of ICG to be loaded on the MSN-Ce6 nanoparticles and to provide a positive surface charge on the nanoparticle. After the surface coating, morphological and size/surface charge analysis was repeated on the so-called MSN-Ce6@PPI nanoparticles to observe the changes of the PPI coating on the nanoparticle. Nanoparticle synthesis was completed with ICG loading, which was the last step of the dual structure nanoparticle synthesis part. After loading different amounts of ICG, the loading capacities of the nanoparticles were determined by performing spectrophotometric analyzes. In addition, surface charge and hydrodynamic diameter analyzes of charged nanoparticles were performed. After the completion of the nanoparticle synthesis part, cell viability analyzes of nanoparticles were performed on healthy fibroblasts and prostate cancer cells. By utilizing the results of the viability analysis, anticancer PDT applications were carried out using the dual laser system and dual nanoparticles at the determined concentrations. In the determined groups, the uptake of nanoparticles into

the cell, the amount of ROS formed, the changes in the mitochondrial membrane potential, the amount of nitric oxide release, the temperature changes during the light applications, the imaging of live/dead cells, and the examination of the nuclear structures of live/dead cells were performed.

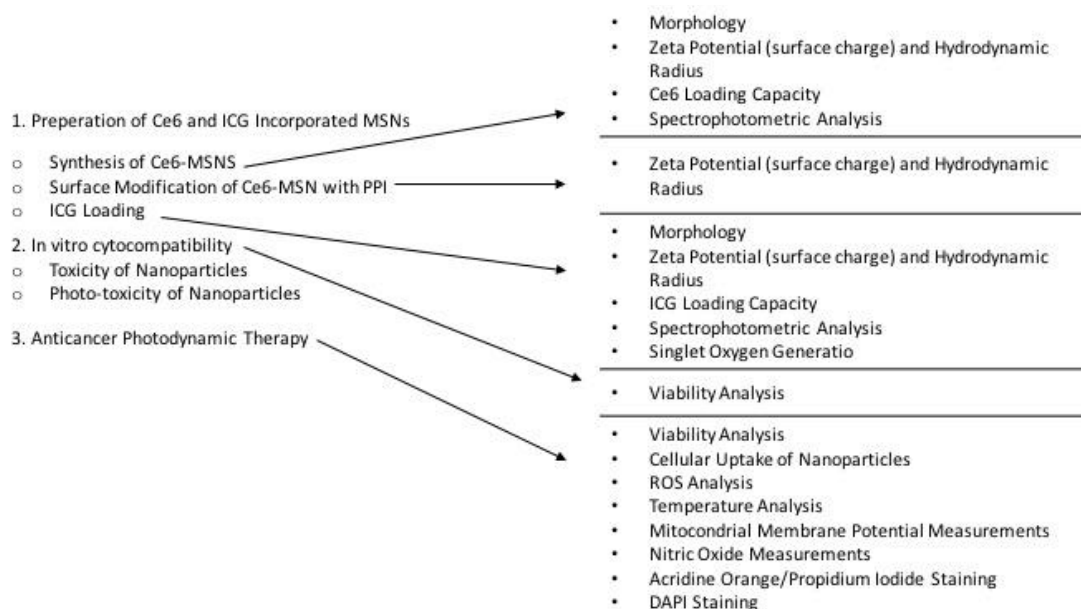


Figure 2: The progress of the study, the methods and, their characterizations

2.1 Cell Culture

PC3 human prostate cancer cell line (ATCC# CRL-1435, Manassas, VA, USA) was used in this current study. The cells were allowed to grow for proliferation in 75-cm² tissue culture flasks in RPMI-1640 solution, containing 1% L-Glutamine, 10% Fetal Bovine Serum solution, and 1% Penicillin-Streptomycin at 37°C and 5% CO₂ humidified atmosphere. The medium was renewed every 2 days for 7 days. Cells incubated for 7 days were found to have a confluency level of 80% and above. Proliferated cells in single layer form were removed from the surface with Trypsin-EDTA 0.05%, containing 0.02% ethylenediaminetetraacetic acid (EDTA) after washing with PBS. To be used in experiments, 10000 cells per well were seeded in a 96-well plate.

L929 fibroblast cells which were supplied from İzmir Kâtip Celebi University Scientific Research Laboratories were grown in 75cm² flasks at 37°C and 5% CO₂ humidified atmosphere to form a single layer. DMEM was used as a growth medium

that was containing 1% L-Glutamine, 10% Fetal Bovine Serum solution, and 1% Penicillin-Streptomycin. The cells reaching the single-layer form were subjected to the above-mentioned trypsinization processes. The cells collected by trypsinization were seeded in 96-well plates, as 10000 cells per well.

2.2 Preparation of Chlorin e6 and Indocyanine Green Incorporated Mesoporous Silica Nanoparticles

2.2.1 Synthesis of MSN with Chlorin e6

Chlorin e6 (Ce6) and indocyanine green (ICG) were used as photosensitizers in this study. Ce6 can absorb light strongly at a wavelength of 414 nm and 650 nm in the absorption band with high efficiency. It also has high stability, but the penetration depth in the tissue is low. ICG can absorb 800 nm of wavelength in the absorption band and has a high penetration depth in the tissue. However, due to its anionic structure, its capacity to enter the cell is low. In addition, photobleaching may occur in the bloodstream in a short time. The positive properties of both photosensitizers were used and the negative properties were eliminated by combining them within the MSN structure. For this reason, dual-structured MSNs have very different properties than those of free photosensitizers alone.

In the preparation of dual structured nanoparticles, tetraethylorthosilicate (TEOS) and hexadecyltrimethylammonium bromide (CTAB) directed to pore formation was used as silica source. Before the synthesis of MSNs, Ce6-APTES reactants were formed. 0,77 mg of Ce6 (1.3 μmol) was dissolved in 500 μl of dichloromethane (DCM), 1 μL of 1-ethyl-3-(3-dimethyl aminopropyl)carbodiimide (EDC) acting as a catalyst was added. The mixture was vortexed until homogenized. Then, 5 μL of aminopropyltriethoxysilane (APTES) was added to the mixture. The reaction was stirred in an inert environment and room temperature for 24 hours to obtain Ce6-Aptes reactant. In the MSN synthesis solution, it was prepared using TEOS: 210 μL , CTAB: 0.04 g, NaOH: 0.01 g, EtOH: 3.6 mL, H₂O: 16 mL. Ce6-APTES reactant was combined with the synthesis solution and TEOS was added. The mixture was left to stir in a dark environment for 24 hours at room temperature. The day after the synthesis

was completed, the solvent extraction of MSN-Ce6 was carried out with 2% (w/v) ammonium nitrate-ethanol solution by applying centrifugation-sonication processes. Ce6-MSNs were dried to be used in the next steps and stored at room temperature. In this way, Ce6 photosensitizer was added to the MSN matrix and named MSN-Ce6.

2.2.2 Surface Modification of MSN-Ce6 with Polypropyleneimine

MSN-Ce6 nanoparticles have been modified with a hyper-branched cationic polypropyleneimine polymer (PPI) by applying the surface augmentation method to eliminate the disadvantage of ICG's anionic characteristics and to increase the loading capacity of ICG. Dry MSN-Ce6 nanoparticles were used in the PPI surface modification process. 50 mg of MSN-Ce6 nanoparticles were placed in a tube and vacuumed for 30 minutes. It was dispersed in 5 mL of toluene at room temperature for 20 min. 5 μ L acetic acid and 30 μ L azeditine were added to it. The solution was left to stir at room temperature for 48h. After 48h, the solution was centrifuged at 4.500 rpm for 5 min at 18°C. The supernatant was removed from the sample and the pellet was dispersed in 8 mL absolute ethanol. Centrifugation (10.000 rpm, 10 min) and sonication were repeated three times, and the pellet was dried and stored in the last step. In this way, PPI polymer was coated on MSN-Ce6 nanoparticles and named MSN-Ce6@PPI.

2.2.3 Indocyanine Green Loading into the Pores of MSN-Ce6@PPI

ICG was loaded into the pores of MSN-Ce6@PPI by solvent immersion method. For this purpose, firstly, 2 mg/mL Ce6-MSN@PPI (4 mg) was dispersed in cyclohexane for 30 minutes with the help of sonication. Then, different amounts of ICG (5%, 7.5%, 10%, 20%) by weight (w/w) of MSN-Ce6@PPI were added and loading was performed. The loading solution was left to stir for 24 h at room temperature and in the dark. The next day, samples that were loaded with different amounts of ICG were collected and allowed to dry. Thus, the production of nanoparticles with different loading rates was completed. The final nanoparticle was named MSN-Ce6@PPI-ICG.

2.3 Physicochemical Characterizations of Nanoparticles

Morphology

Scanning Electron Microscopy (SEM) analysis was used to analyze and visualize the shape and size of the nanoparticles as a morphology analysis. SEM analysis enables the magnification of the solid inorganic materials desired to be imaged using electron beams. SEM was used to visualize the nanoparticles that are prepared in this study. The samples were dried and coated with gold before the analysis. The SEM device which is present in the Scientific Research Laboratories of İzmir Kâtip Celebi University was used to carry out the analysis as service procurement.

Hydrodynamic Radius and the Zeta Potential analysis of Nanoparticles

The hydrodynamic particle size and net surface charge of nanoparticles were measured using dynamic light scattering (DLS). Nanoparticles were prepared for the measurements by dispersing from the dry state to get the determined concentrations in HEPES. Measurements were made in the Scientific Research Laboratories of İzmir Kâtip Celebi as service procurement.

ICG Loading Capacity Analysis of the Nanoparticles

The absorption capacities and spectrum characteristics of ICG and Ce6 were investigated before and after loading into the nanoparticles. Before loading, Ce6 and ICG were dispersed in HEPES at determined concentrations and an absorption standard curve was created using a microplate reader (Multimode Microplate Reader Biotek Synergy HTX, Biotec). Absorption capacities and characteristics after loading the photosensitizers into the nanoparticle were investigated again using the microplate reader. For Ce6, nanoparticle solutions were prepared at certain concentrations, after spectroscopic analysis, the amount of Ce6 loaded was determined by applying the absorbance values on the standard curve. For ICG, the absorbance values obtained by

using a microplate reader as a result of the leaching method were used on the standard curve, and the amount of ICG loaded into the nanoparticle was measured.

Determination of Singlet Oxygen Generation Capacity of the Nanoparticles

Singlet oxygen generation capacity of MSN-Ce6@PPI-ICG nanoparticles with dual laser excitation was determined using 1,3-diphenylisobenzofuran (DPBF). In the presence of singlet oxygen, DPBF decomposes to 1,2-dibenzoylbenzene. DPBF initially has a very strong absorption band at 415nm wavelength, and the reduction in the absorption capacity at this wavelength is directly proportional to the amount of singlet oxygen formed. 8 mM (4uL) DPBF was added to nanoparticles prepared in 200 μ L DMSO at concentrations of 10, 25, 50, 100, 200, and 400 μ g/ml. Absorption spectra were taken using a microplate reader before dual laser application. Dual laser application was performed to the same nanoparticle samples, and absorption spectrum measurements were taken after the light application. The amount of decrease in absorption at 415 nm of wavelength was correlated with the amount of singlet oxygen generated.

2.4 Light Sources and Dual Optical System

Diode lasers emitting at 655-nm (PS4 III. LED; Changchun New Industries Optoelectronics Tech. Ltd., China) and 808-nm (Teknofil, Istanbul, Turkey) of wavelengths were used as the light sources. It was aimed to stimulate Ce6 with 655-nm red laser light and ICG with 808-nm near-infrared laser light. The 655-nm diode laser device has optical fiber output, with a maximum output power of 1W and a continuous mode of irradiation. The 808-nm diode laser device has a 2W maximum output power and has optical fiber output. It can irradiate in continuous and pulsed mode. The dual laser design was built by using these two laser devices. The light coming from two different laser devices was overlapped at one point and the application area on a 96-well plate was tried to be illuminated simultaneously.

$$\text{Energy Density (J/cm}^2\text{)} = \text{Power (W)} / \text{Area (cm}^2\text{)} \times \text{Time}$$

As it can be seen in the Figure 2.4, the design of lasers was built on the optical table. Optical fibers with a diameter of 400 μm compatible with both devices were placed perpendicular to the optical table with various optomechanical instruments. The optical fiber connected to the 655-nm diode laser device was placed at a distance of 9 cm, and the 808-nm diode laser was placed at a distance of 12 cm from the optical table. With this setup, a circular area of 0,75 cm in diameter and 1.767 cm^2 in the area was created on the 96-well plate, illuminating the 4 wells equally. The output powers were set as 300 mW and 600 mW for the 655-nm and 808-nm diode lasers, respectively. The time-dependent energy densities were calculated according to the formula used above. With simultaneous application of light for 706 seconds, energy densities of 120 J/cm^2 for 655-nm diode laser and 240 J/cm^2 for 808-nm diode laser were obtained. The dual structured nanoparticle was excited simultaneously with the light coming from both lasers.

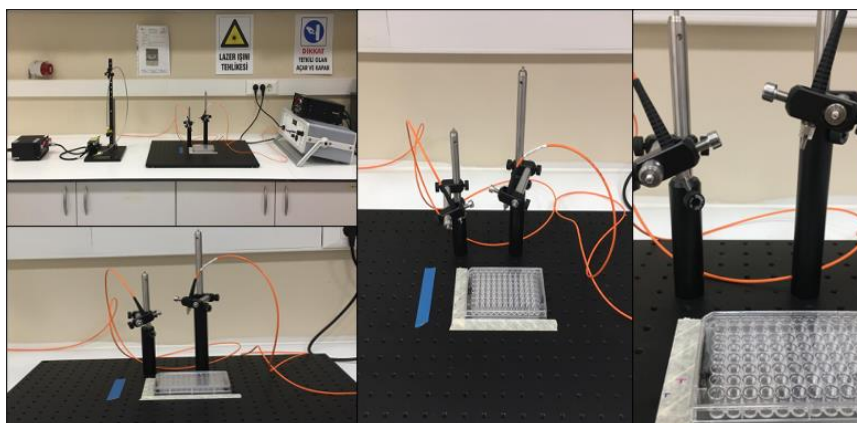


Figure 2.4: Dual Laser Optical System

2.5 Experimental Groups

The cells were incubated for 24 hours at 37°C and 5% CO₂ humidified atmosphere after seeding them to adhere to the 96-well plate surface. Experimental procedures were then applied. Dual nanoparticle and light applications were taken into consideration while creating the experimental groups. After a certain incubation period at 37°C and a 5% CO₂ humidified atmosphere, a dual-laser application was performed on groups containing dual nanoparticles or photosensitizers. The groups that did not contain dual nanoparticles or photosensitizers were incubated with the growth medium to provide equal conditions and necessary procedures were applied. After incubation

at 37°C and 5% CO₂ humidified atmosphere, all groups were washed with PBS and a fresh medium was added. The light application was applied to the groups that included dual-laser applications. Experimental groups were:

-Control: Light or dual nanoparticles were not applied

-Laser group: only dual-laser was applied

-Dual MSNs group: only dual-nanoparticle was applied

-Free Ce6 & ICG group: Free Ce6 & ICG was applied with the same amount that was present in the structure of the dual-nanoparticle

-PDT with free Ce6 & ICG: dual-laser was applied after the incubation of free Ce6 & ICG with the same amount that was present in the structure of the dual-nanoparticle

-PDT with Dual MSNs group: the dual-laser application was performed after the incubation with dual-structured MSN

2.6 In Vitro Analysis

2.6.1 Cytotoxicity Investigations of the Nanoparticles on PC3 Prostate Cancer and L929 Fibroblast Cells

3-(4,5-dimethyliazol-2-yl)- 2,5-diphenyl tetrazolium bromide (MTT) was used to determine cellular viability. MTT initially has a yellow color. This yellow color turns purple when it interacts with the enzyme succinate dehydrogenase, which is found in the mitochondria of living cells and has a direct relationship with mitochondrial activity. The absorbance of this purple color is used to directly express the mitochondrial activity and indirectly to quantitatively express cell viability.

After any applications to determine the cell viability and cyto/phototoxicity, an MTT assay was used. First of all, MTT stock solution was prepared at a concentration of 5 mg/mL in distilled water. The media were removed from the groups in which the experimental procedure was applied. Using the stock solution, 100 µL of MTT solution was added to each well of the 96-well plate with 10% MTT and 90% serum-

free medium. Cells were incubated in this solution for 2 hours at 37°C and 5% CO₂ humidified atmosphere in the dark. After incubation, MTT solutions were removed and 100 µL DMSO was added. The absorbance of purple color was measured at 570 nm by a microplate reader (Multimode Microplate Reader Biotek Synergy HTX, Biotec). In all stages of MTT assay were performed at dark.

To examine the cytotoxicity of MSN-Ce6@PPI-ICG nanoparticles on PC3 cells, different concentrations of MSN-Ce6@PPI-ICG nanoparticles were applied, varying from 1 µg/ml to 400 µg/mL concentrations. After the nanoparticles were dispersed in RPMI-1640, they were incubated with PC3 cells with two different incubation times of 4 hours and 24 hours. After incubations, the nanoparticle solutions were removed from the cells and the cells were washed with PBS. After removing all the nanoparticles that were not taken into the cell, the viability of the cells was determined by the MTT analysis as described above.

In addition, the cytotoxicity of MSN-Ce6@PPI-ICG nanoparticles on L929 healthy fibroblast cells was investigated. MSN-Ce6@PPI-ICG nanoparticles at 25, 50, and 100 µg/mL concentrations were incubated with L929 cells for 24 hours, and excess nanoparticles were removed by washing. After the incubation of 24 hours, the cell viability was determined immediately at first and then 24 hours after the applications, by the MTT assay as described above.

2.6.2 Photo-Toxicity Analysis of the Nanoparticles on PC3 Prostate Cancer and L929 Fibroblast Cells after PDT Applications

Phototoxicity studies were carried out in PC3 cancer cells by excitation of MSN-Ce6@PPI-Ce6 nanoparticles with a dual laser system. MSN-Ce6@PPI-Ce6 nanoparticles at concentrations of 5, 10, 25, 50, and 100 µg/mL were dispersed in the growth medium and then incubated with PC3 cells for 4 and 24 hours. After the incubation period ended, the excess nanoparticles were removed by washing with PBS. After the growth medium was added to the cells, the laser applications were performed with the dual laser optical system. Immediately after the applications, the metabolic activities of the cells were measured with the MTT analysis described in 2.6.1.

Phototoxicity of MSN-Ce6@PPI-Ce6 nanoparticles was also investigated on L929 cells. Selected nanoparticle concentrations of 25, 50, and 100 $\mu\text{g/ml}$ were determined by dispersing them in the growth medium. Nanoparticles were incubated with L929 cells for 24 hours. At the end of the incubation period, excess nanoparticles were removed by washing with PBS. After the addition of the growth medium, laser application was performed with the dual laser optical system. To see the long-term effect of anticancer activity on healthy cells after the application, MTT analysis was performed 24 hours after the laser application.

2.7 Cellular Uptake of Nanoparticles into PC3 Cells

Triton-100X was used to study the penetration of nanoparticles into PC3 prostate cancer cells. Cells were seeded onto the 96-well plate at 10^4 cells per well. Cells were incubated with nanoparticles at concentrations of 25, 50, and 100 $\mu\text{g/mL}$ for 24 hours at 37°C and 5% CO_2 humidified atmosphere in the dark. After the nanoparticle solutions were removed from the cells after incubation, the cells were treated with 30% Triton-100X prepared with DMSO and ethanol. Afterward, the absorption spectra were analyzed using a multiplate reader.

2.8 Analysis of the Intracellular ROS Production in PC3 Cells after PDT Applications

2',7'-dichlorofluorescein diacetate (DCFH-DA) was used to analyze the intracellular ROS generation after the applications. DCFH-DA is a non-fluorescent compound that can be converted into a fluorescent compound, dichlorofluorescein (DCF), in the presence of ROS. The amount of DCF in the presence of ROS can be directly correlated with the amount of ROS produced. First, a starting stock solution of DCFH-DA was prepared at 40 mM in DMSO. This stock solution was diluted to a concentration of 0.1 mM using an RPMI-1640 growth medium containing 1% FBS. In designated groups, before performing the experimental procedures, cells were incubated with 0.1 mM DCFH-DA solution for 1 hour at 37°C and 5% CO_2 humidified atmosphere in the dark and washed twice with phosphate-buffered saline (PBS) to remove any DCFH-DA that did not enter the cells. Cells were then treated with dual-

nanoparticles and/or laser light. At the end of the applications, the fluorescence intensity of DCF fluorescence was measured with a multiplate reader immediately after the applications using the excitation wavelength of 485/20 nm and the emission wavelength of 528/20 nm. All steps of the analysis were performed in the dark.

2.9 Analysis of the Mitochondrial Membrane Potential Change in PC3 Cells after PDT Applications

Mitochondrial membrane potential changes during light and nanoparticle applications were determined with the JC-1 Mitochondrial Membrane Potential assay kit. Before applying the nanoparticle to the cells, they were washed with PBS and incubated with 10 μ M JC-1 solution for 30 minutes. At the end of the incubation, the cells were washed 2 times with PBS and the specific application procedures of each group were completed. Immediately after the applications, emission values at 535 nm of wavelength for a red fluorescence and 595 nm of wavelength for green fluorescence were obtained with the excitation at a wavelength of 475 nm using a microplate reader (CLARIOstar Microplate Reader BMG LABTECH, Germany). After fluorescence values of mitochondrial membrane changes were obtained, microscopic images were taken with fluorescence microscopy (Olympus CKX41, Olympus Co. Ltd., Tokyo, Japan). These images were obtained using CellSens Imaging Software and represented hyperpolarization in mitochondrial membrane potential in live cells emitting red fluorescence.

2.10 Analysis of the Nitric Oxide Release in PC3 Cells after PDT Applications

The amount of nitric oxide (NO) released as a result of nanoparticle and dual laser application was measured using Griess Reagent containing sulfanilic acid and N-(1-naphthyl)ethylenediamine. Nitrite molecules, the decomposition product of NO, react with sulfanilic acid and N-(1-naphthyl)ethylenediamine to form a dye molecule that can be determined spectrophotometrically. One hour after the specific dual laser and nanoparticle applications of the experimental groups were completed, samples were taken from the supernatant of the cells. This supernatant was combined with the same

amount of Griess Reagent solution and the samples were incubated for 30 minutes. After incubation, the absorbance values were measured with a microplate reader at a wavelength of 548 nm. The values were plotted according to the equation obtained from the standard curve of standard nitrite solution prepared at different concentrations. The obtained absorbance values were used to calculate the amount of nitrite molecules, which is the breakdown product of NO, formed in each experimental group and these values are also directly proportional to NO released after each application.

2.11 Live/Dead Cell Analysis via Acridine Orange/Propidium Iodide Staining of PC3 Cells after PDT Applications

In this study, the acridine orange/propidium iodide (AO/PI) staining was used to visualize live and dead cells. Acridine orange is a weak base (an inclusion dye) that can easily penetrate live cells. It glows green with intact or condensed nuclei in living or early apoptotic cells into which it enters. Propidium iodide (exclusion dye) cannot enter living cells, but it glows red with intact or condensed chromatin in dead or late apoptotic cells. This red light generates directly related information about the free DNA content. The AO/PI solution was diluted at 1:10 with PBS for use in the experiments. After performing the experimental procedures, the media was removed from the cells and the cells were washed with the same volume of PBS. Dye was added to each well in the 96-well plate, 3 μ l AO/PI dye, and 27 μ l PBS. It was incubated for 30 min at 37°C and 5% CO₂ humidified atmosphere. The images were taken with a fluorescence microscope using CellSense Entry software. In the images, the green color represented live cells, while the red color represented dead cells.

2.12 Apoptosis Analysis via DAPI Staining in PC3 Cells

4',6-diamidino-2-phenylindole (DAPI) chemical binds to the double-stranded DNA structure in the cell nucleus and emits blue light. It is mainly used to label the DNA of cells. It is also used to visualize different nuclear morphological changes such as chromosome condensation or fragmentation in apoptotic cells. In this study, a DAPI

application was made for this purpose. After the experimental procedure in which dual nanoparticles and light were applied to the cells in the 96-well plate, the medium was removed. Cells were fixed with 4% paraformaldehyde for 5 min at 37°C and 5% CO₂ humidified atmosphere. After washing once with sterile PBS, DAPI solutions were added to each well at a concentration of 10 µg/ml. After 20 minutes of incubation at 37°C and 5% CO₂ humidified atmosphere, they were washed with PBS and viewed with a fluorescent microscope.

2.13 Temperature Measurements

During laser application, there is an energy transfer from light and this energy can cause an increase in the temperature in the environment. In addition, the nanoparticles used can cause an extra temperature increase. Since the temperature increase exceeds a certain point, photothermal effects may play a role and side effects can be seen related to high temperature. In this study, cell death was targeted by the PDT mechanism via photochemical processes. Temperature measurements were carried out at certain time intervals during light applications to determine that cell death was not via photothermal, but via ROS-mediated photodynamic therapy without a significant temperature rise. Temperature measurements were performed with the help of a thermal camera (Testo, Thermal imager) in the PDT groups applied with the determined nanoparticle concentrations and only the laser group.

2.14 Statistical Analysis

All experiments were repeated three times with three samples in each experiment. Statistical analysis was performed with GraphPad Prism Version 9.0.1 (GraphPad Software Inc., La Jolla, CA, USA). At first, the data were analysed with one-way analysis of variance (ANOVA). Afterwards, Tukey post hoc test was used to see the statistically significant results between the control and experimental groups. A *p* value less than 5% was considered statistically significant.

Chapter 3

Results and Discussions

3.1 Preparation of MSN-Ce6@PPI-ICG Nanoparticles

3.1.1 Synthesis of MSN-Ce6 Nanoparticles Morphology of MSN-Ce6 Nanoparticles

Morphological examination of MSN nanoparticles was performed by SEM analysis. Since Ce6 was included in the structure of MSN nanoparticles during the production phase and was in the matrix structure, the morphological examination was performed on this nanoparticle group. It has been observed that nanoparticles have average sizes in spherical and non-aggregate forms (Figure 3.1.1). In addition, it was understood that Ce6 did not cause any change in nanoparticle size and shape.

Net Surface Charge and Hydrodynamic Radius of MSN-Ce6 Nanoparticles

As a result of the zeta analysis of the generated MSN-Ce6 nanoparticles, the net surface charge was determined as 16 ± 0.07 mV. According to the average hydrodynamic diameter analysis, the nanoparticles had an average hydrodynamic diameter of 1052 ± 149.5 nm. The PDI value showing the ability to be dispersed is 0.044 ± 0.032 , and because it is less than 0.1, it shows that it is monodisperse (Figure 3.1.1)

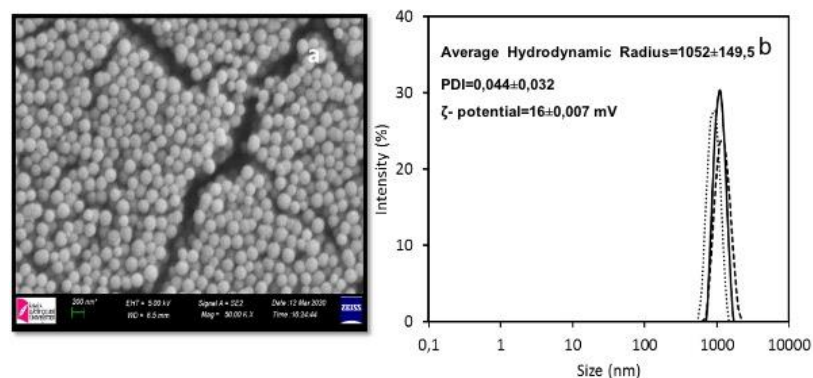


Figure 3.1.1: a) SEM image of MSN nanoparticles produced with Ce6 photosensitizer. b) Size distribution, average hydrodynamic diameter, PDI value and Zeta potential data of 0.2 mg/mL Ce6-MSN prepared in HEPES buffer solution (pH 7.2, 25 mM).

Loading Capacity of MSN-Ce6 Nanoparticles

Spectrophotometric analyzes were used to determine the amount of Ce6 loaded into the MSN matrix. First of all, the absorbance spectrum of solutions containing only ICG and only Ce6 at 2.5 $\mu\text{g/mL}$ concentration were examined. According to the data obtained; Specifically, Ce6 showed higher absorbance at 414 nm and 650 nm of wavelengths, ICG showed higher absorbance at 780 nm of wavelength (Figure 3.1.1.a.a.). Later, ICG and Ce6 photosensitizers were combined to correspond to the same concentration and it was understood that they did not affect each other's specific absorbance and spectrophotometric properties. In addition, a calibration curve was created with absorbance values corresponding to increasing Ce6 and ICG concentrations (Figure 3.1.1.a.b.).

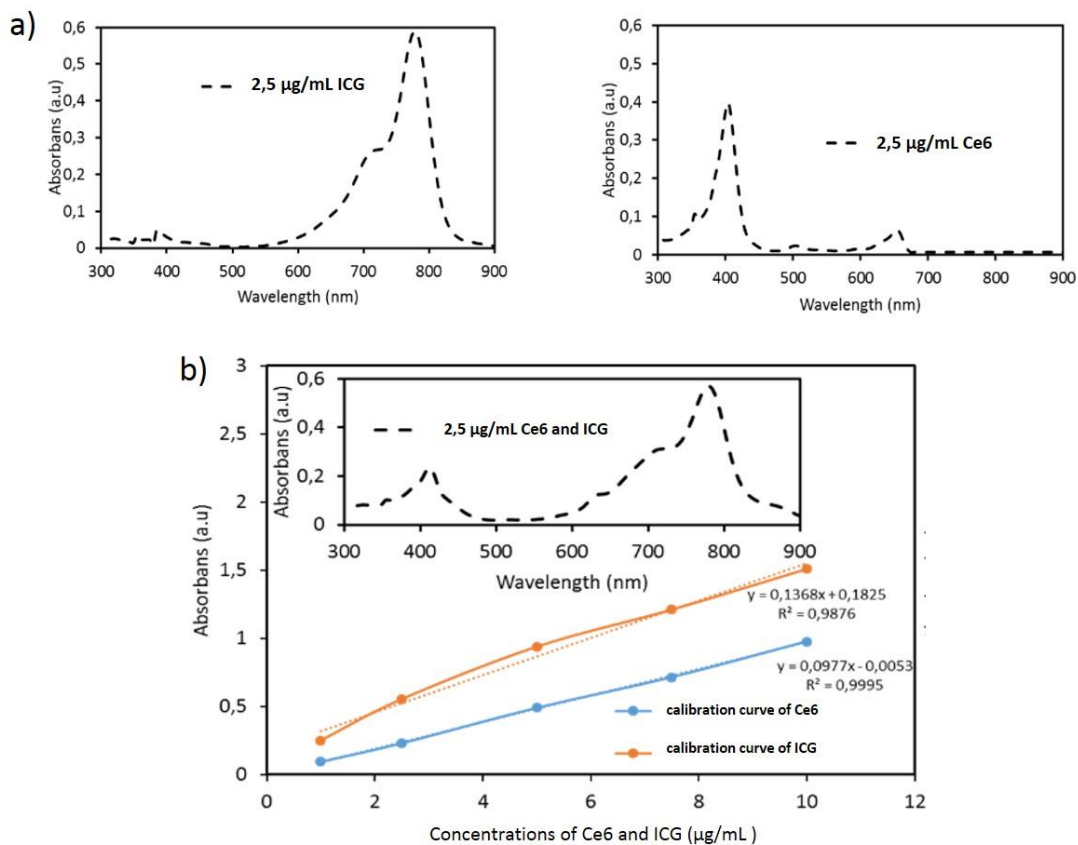


Figure 3.1.1.a: a) Absorbance Spectrum of 2.5 µg/mL Ce6 and ICG photosensitizer b) The absorbance values corresponding to the increasing concentrations of Ce6 and ICG photosensitizers and the obtained calibration curves, Inset figure; absorbance spectrum of the combined solution of free 2.5 µg/mL Ce6 and ICG photosensitizers.

The loading amount of Ce6 to the MSN nanoparticle was determined as 2.4% by processing the absorbance values obtained after dispersing the MSN-Ce6 nanoparticles in the HEPES solution on the calibration curve.

3.1.2 PPI Surface Modification of MSN-Ce6 Nanoparticles

Net Surface Charge and Hydrodynamic Radius of MSN-Ce6@PPI Nanoparticles

The resulting Ce6-MSN nanoparticles were surface modified with cationic polypropylene imine polymer (PPI). The results of Zeta Potential and DLS analyzes are given in Table 3.1.2. According to these values, it was observed that PPI-coated MSN-Ce6 nanoparticles (MSN-Ce6@PPI) had low hydrodynamic diameter with good

colloidal stability. It was determined that the zeta potential of PPI-coated nanoparticles was higher than MSN-Ce6 nanoparticles. It was predicted that this would be advantageous in the next loading of the anionic ICG. This was indicated good colloidal stability. According to the obtained PDI value, MSN-Ce6@PPI nanoparticles were also found to be monodispersed because it was close to 0.1. As a result of the thermogravimetric analysis, it was determined that 28% by mass of the nanoparticle was coated with PPI.

Table 3.1.2: Zeta Potential and DLS results before and after surface modification

	ζ - Potential (mV)	Average Hydrodynamic Radius (nm)	PDI	
MSN-Ce6	16±0.07	1052±149.5	0.044±0. 032	
MSN- Ce6@PPI	46.8±1.22	651.2±16.93	0.13±0.03	

It has been reported that MSN nanoparticles with PPI dendrimers provide a high amount of cargo agents. In addition, it was reported in the same study that PPI dendrimers successfully closed the MSN pores and prevented the early release of cargo molecules in the MSN [78]. In our study, by coating MSN-Ce6 nanoparticles with PPI, the early release of loaded Ce6 was prevented, the amount of ICG loaded into the pores in the next step was increased, and the early release of ICG was prevented.

3.1.3 ICG Loading to the MSN-Ce6@PPI Nanoparticles

Net Surface Charge and Hydrodynamic Radius of MSN-Ce6@PPI Nanoparticles

The analysis of the net surface charge, average hydrodynamic diameter and size distribution of the nanoparticles was repeated to see that the different amounts of ICG loading did not cause a negative effect on the nanoparticle structure like structural damage. As a result of the obtained data, it was understood that all nanoparticles with different ICG loading ratios were dispersible. Except for the group with 5% initial loading amount, the groups with another loading amount showed negative surface charge (Table 3.1.3a). It has been proven that the surface charge of cancer cells is negative due to the high glycolysis ratio, and the surface charge of normal cells is slightly positive or neutral. In addition, it was shown in the same study that the positively charged nanoprobe formed strongly bind to cancer cells, and normal cells were ineffective to nanoprobe [79]. For this reason, the positive charge of nanoprobe used for diagnostic or therapeutic purposes and the selectivity of nanoprobe to cancer cells are important. In our study, with this idea, the MSN-Ce6@PPI-ICG nanoparticle with an initial ICG charge of 5% and a positive surface charge was advantageous. The selectivity of these nanoparticles in cancer cells over normal fibroblast cells was demonstrated in the viability analysis. Compared to healthy cells, cancer cells showed higher mortality rates at the same nanoparticle concentrations and light dose of dual lasers. These results confirm the proposed idea. In addition, the known disadvantages arising from the anionic structure of ICG have been eliminated by PPI coating and this is explained by the positive surface charge of the final MSN-Ce6@PPI-ICG(5%) nanoparticles. For these reasons, this group was preferred in other analysis methods and *in vitro* PDT applications.

Table 3.1.3a: Zeta Potential and DLS results of MSN-Ce6@PPI-ICG nanoparticles with different loading rates

Name	ζ - Potential (mV)	Average Hydrodynamic Radius (nm)	PDI
Ce6-MSN@PPI	46.8±1.22	651.5±16.93	0.13
Ce6-MSN@PPI-ICG (%5)	20.5±0.40	349.4±2.9	0.28
Ce6-MSN@PPI-ICG (%7.5)	-35.3±0.40	301.6±6.88	0.2
Ce6-MSN@PPI-ICG (%10)	-38.6±0.95	266.1±1.21	0.25
Ce6-MSN@PPI-ICG (%20)	-32.5±0.92	231.5±0.513	0.18

Loading Capacity of MSN-Ce6@PPI-ICG Nanoparticles

MSN-Ce6@PPI nanoparticles were loaded with different amounts of ICG by mass. The initial loading amount and the loaded amount were calculated with the help of the calibration curve and absorbance values. As a result of the loadings, ICG loading amounts were calculated to be in the range of 1-10 $\mu\text{g/mL}$. Also, it was observed that the loading amount of ICG increased as the initial loading amount increased in MSN-Ce6 and MSN-Ce6@PPI nanoparticles. In addition, the same amount of ICG was loaded on MSN-Ce6 nanoparticles with the same method in order to see the role of

PPI polymer in ICG loading. As seen in the Table 3.1.3b, it was understood that the PPI coating increased the ICG loading capacity on MSN-Ce6 nanoparticles.

When the sample with the highest amount of ICG, Ce6-MSN@PPI-ICG (20) (initial ICG amount was 20% w/w), was analyzed by spectrophotometric measurement, the spectrum given below was obtained (Figure 3.1.3) In this way, it was observed that the strategy applied did not cause any structural damage as it showed a similar spectrum to both free ICG and Ce6 solutions. That is, the wavelengths that give the maximum absorbance value at specific wavelengths of ICG and Ce6 did not change before and after loading.

Table 3.1.3b: Amount of ICG loaded on MSN-Ce6 and MSN-Ce6@PPI nanoparticles

Initial Loading of ICG (mass ratio of Ce6-MSN % w/w)	Amount of Loaded ICG to Ce6-MSN (%w/w)	Amount of Loaded ICG to Ce6-MSN@PPI (%w/w)
5	0.4	0.9
7.5	1.5	4.9
10	4.3	15.7
20	6.2	24.2

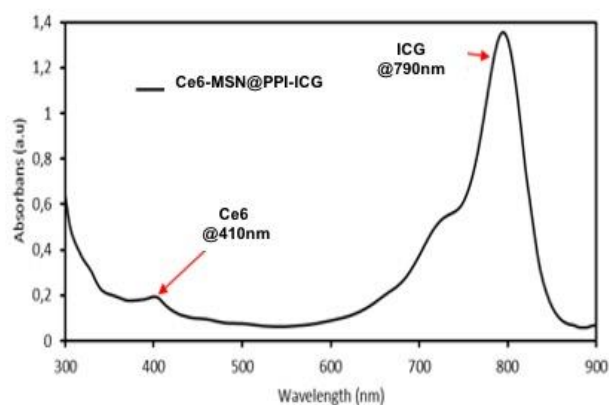


Figure 3.1.3: Absorbance spectrum of 0.1 mg/mL Ce6-MSN@PPI-ICG(20) in DMSO and the initial loading amount of ICG is 20%.

3.2 Singlet Oxygen Generation Capacity of MSN-Ce6@PPI-ICG Nanoparticles

The capacity to form singlet oxygen of the MSN-Ce6@PPI-ICG nanoparticle with an initial ICG loading rate of 5% was investigated. For this process, DPBF chemical known as singlet oxygen probe was applied to MSN-Ce6@PPI-ICG (5%) nanoparticles at 10, 25, 50, 100, 200, and 400 $\mu\text{g/mL}$ concentrations and their free photosensitizer groups. The amounts of singlet oxygen formed by nanoparticles were determined before and after the application of the dual laser optical system (655-nm diode laser: 300 mW output power, 120 J/cm^2 energy dose, 706 seconds application time, 808-nm diode laser: 600 mW output power, 240 J/cm^2 energy dose, 706 seconds) planned to be used in the experiments. As it can be seen (Figure 3.2a), the nanoparticle with the highest singlet oxygen generation capacity was the nanoparticle with a concentration of 200 $\mu\text{g/mL}$. When light was applied to the ICG and Ce6 photosensitizers in the free form in the structure of the nanoparticle at these concentrations, the amount of singlet oxygen formed with the increasing concentration also increased, as predicted for 10, 100, 200, 400 $\mu\text{g/mL}$ (Figure 3.2b). However, this was not observed when photosensitizers were in nanoparticle structure. Although an increase was observed up to 200 $\mu\text{g/mL}$ concentration, the amount of singlet oxygen obtained when light was applied to the nanoparticle at 400 $\mu\text{g/mL}$ concentration was less than that obtained at 100 and 200 $\mu\text{g/mL}$. This showed that the singlet oxygen generation capacity of the nanoparticle did not change after a certain point. MSN-

Ce6@PPI-ICG nanoparticles showed that the singlet oxygen generation capacity was full after 200 $\mu\text{g/ml}$ concentration. MSN-Ce6@PPI-ICG nanoparticles showed that the singlet oxygen generation capacity was full after 200 $\mu\text{g/ml}$ concentration. For this reason, we planned to create lower concentrations for in vitro studies and examined the singlet oxygen generation capacity of 25, 50, 100 $\mu\text{g/ml}$ concentrations. When the DPBF analysis of 25, 50, and 100 $\mu\text{g/ml}$ nanoparticles selected at low concentrations was examined as a spectrum before and after dual laser application, it has also shown that the singlet oxygen forming capacity of the nanoparticle increased at low concentrations as the concentration increased (Figure 3.2c).

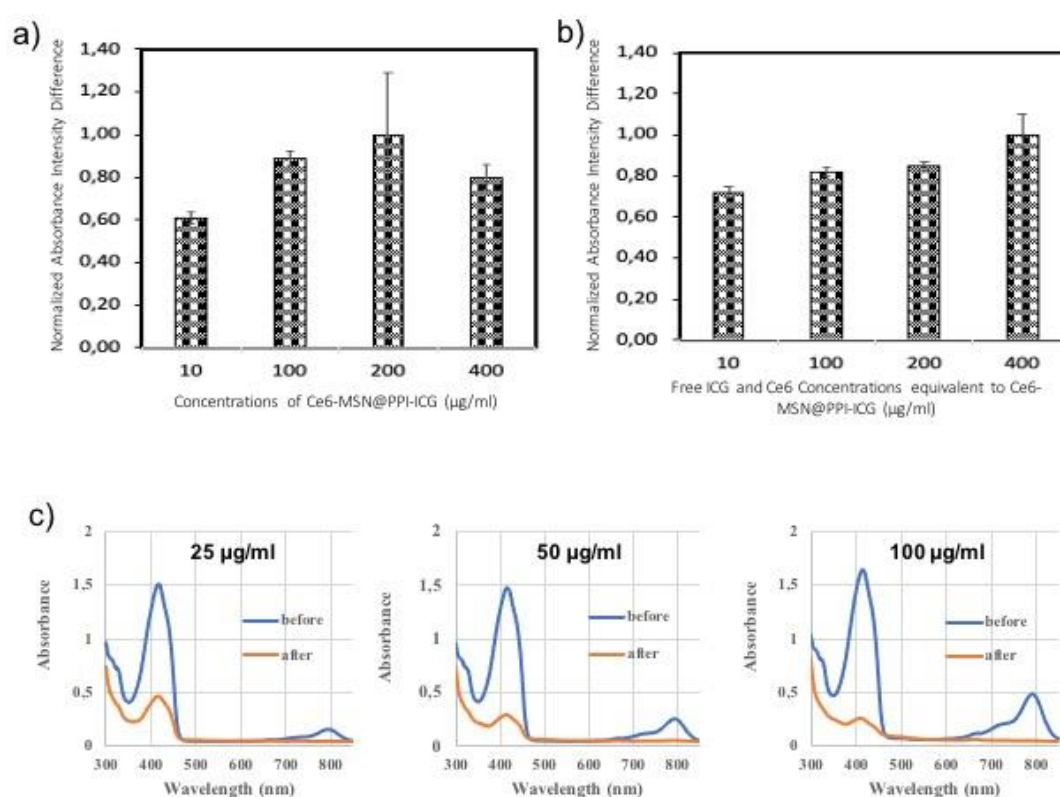


Figure 3.2. a) Singlet oxygen ratio of Ce6-MSN@PPI-ICG(5%) at different concentrations before and after stimulation with dual laser optic system b) singlet oxygen ratio of free photosensitizers before and after stimulation with dual laser optic system (for 10 $\mu\text{g/mL}$ nanoparticle: 0.24 $\mu\text{g/mL}$ Ce6 and 0.045 $\mu\text{g/mL}$ ICG, for 100 $\mu\text{g/mL}$ nanoparticle: 2.4 $\mu\text{g/mL}$ Ce6 and 1.8 $\mu\text{g/mL}$ ICG, for 200 $\mu\text{g/mL}$ nanoparticle: 4.8 $\mu\text{g/mL}$ Ce6 and 3.6 $\mu\text{g/mL}$ ICG, for 400 $\mu\text{g/mL}$ nanoparticle: 9.16 $\mu\text{g/mL}$ Ce6 and 7.2 $\mu\text{g/mL}$ ICG) c) 25, 50, and 100 $\mu\text{g/mL}$ nanoparticle DPBF spectrum of Ce6-MSN@PPI-ICG(%5) nanoparticles before and after dual laser optic system. The samples were carried out for DBPF analysis in DMSO and the initial loading amount of ICG is 5%.

3.3 Viability Analysis

3.3.1 MTT Analysis

Cytotoxicity of MSN-Ce6@PPI-ICG Nanoparticles in PC3 Cells

Toxicity studies of MSN-Ce6@PPI-ICG nanoparticles on PC3 cancer cells were performed by MTT analysis. Here, it was aimed to determine the optimum incubation time as well as the toxicity of nanoparticles. For this reason, nanoparticles at 1, 5, 10, 25, 50, 100, and 400 $\mu\text{g/mL}$ concentrations were added onto PC3 cancer cells and incubated with incubation times of 4h and 24h. Viability analysis results obtained as a result of incubation times were shown (Figure 3.3.1a). The obtained data were expressed as a percentage change by dividing it with the data of control group. Looking at the results, after 4h incubation period, 1, 5, 10, 25, 50, and 100 $\mu\text{g/mL}$ concentrations showed 92.74%, 99.8%, 92.62%, 103.26%, 96.66%, and 93.44% cell viability, respectively. In the group where 4h incubation time was used, the maximum concentration of 400 $\mu\text{g/mL}$ nanoparticle application showed 72.66% cell viability of PC3 cancer cells. All nanoparticle concentrations using 4h incubation did not cause significant cytotoxicity on PC3 cells. As a result of the statistical analysis, no significant results were found in all nanoparticle groups in which 4h incubation time was used. Statistical analysis data also showed that 4h incubation of these concentrations were not toxic to PC3 cancer cells.

In the viability analysis using nanoparticles at the same concentrations on PC3 cancer cells, 1, 5, 10, 25, 50, and 100 $\mu\text{g/mL}$ nanoparticles were 94.56%, 102.17%, 95.69%, 92.86%, 84.11%, and 73.34%, respectively, according to the 24h incubation time results. The highest concentration of 400 $\mu\text{g/mL}$ nanoparticles resulted in 23.4% cell viability. When the results were examined, it was seen that after the 25 $\mu\text{g/ml}$ nanoparticle concentration increased cellular death was seen at increasing concentration. 25, 50, 100, 400 $\mu\text{g/ml}$ of concentrations caused subsequent cellular damage on PC3 cancer cells. When the results were analyzed statistically, the groups in which this cellular damage was statistically significant were the MSN100 and

MSN400 groups. That is, MSN-Ce6@PPI-ICG nanoparticles were toxic on PC3 cells at a concentration of 100 and 400 $\mu\text{g/ml}$ after 24h incubation time.

In general, when the groups using 4h and 24h incubation times were compared, the results of 24h incubation time caused more significant cellular damage on PC3 cells than the results of 24h incubation time. This showed that nanoparticles were more taken into the cell after 24h.

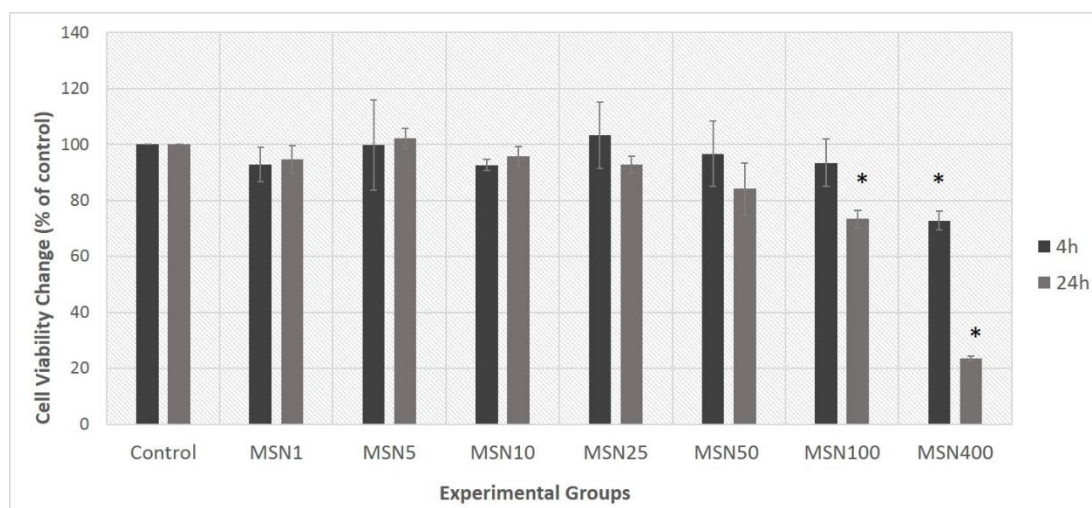


Figure 3.3.1a: Cell viability of 1, 5, 10, 25, 50, 100, 400 $\mu\text{g/mL}$ MSN-Ce6@PPI-ICG (%5) nanoparticles after the 4h and 24h incubation time on PC3 cells. Statistically significant results are represented with * ($P < 0.05$).

Cytotoxicity of MSN-Ce6@PPI-ICG Nanoparticles in L929 Cells

Viability analyzes were performed on L929 to see the toxicity of MSN-Ce6@PPI-ICG nanoparticles on healthy cells. Taking into account the results of the viability analysis performed on PC3 cancer cells, nanoparticles at 25, 50, and 100 $\mu\text{g/mL}$ concentrations were selected. After the 24h incubation period was found to be appropriate for PDT applications, the viability results were shown after the 24h nanoparticle incubation time. 0h results are represented viability immediately after the applications. 24h results represented the viability 24h after the applications. Looking at the 0h result; 25, 50, and 100 $\mu\text{g/mL}$ nanoparticles showed 107.88%, 88.26%, and 80.9% viability, respectively. As expected, the viability rate decreased as the nanoparticle concentration increased. According to the results of the statistical analysis, the decreases in vitality were not found to be statistically significant except for the

MSN100 nanoparticle group. To examine the long-term effects of nanoparticles after the application, the results of the viability analysis 24h after the application were given. According to the results, an increase in viability was observed in the 50 and 100 ug/ml nanoparticle groups compared to the 0h results. When the results were examined, the MSN100 group was found to be statistically significant. Ziemba et al. showed that PPI dendrimers are toxic [80]. For this reason, it was an expected result that the MSN100 group would have a toxic effect on healthy cells. Also, it was shown that there was no permanent damage to healthy cells after other nanoparticle applications (Figure 3.3.1b). The increase in cell viability is proof that the damage caused by nanoparticle application in healthy cells is started to be repaired in a short time and the cells started to proliferate again when they completed their cell cycle.

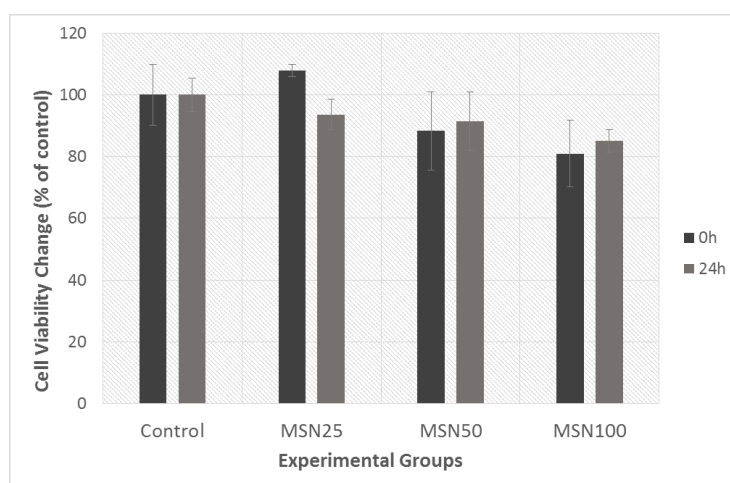


Figure 3.3.1b: Cell viability of 25, 50, and 100 $\mu\text{g/mL}$ MSN-Ce6@PPI-ICG (%5) nanoparticles at immediately after applications and 24h after the applications on L929 cells. Statistically significant results are represented with * ($P < 0.05$).

Phototoxicity of MSN-Ce6@PPI Nanoparticles in PC3 Cells

The photo-toxicity analysis of PDT groups in which dual laser application was performed with nanoparticles on PC3 cancer cells was performed (Figure 3.3.1c). 4h and 24h incubation times were also used in PDT groups to see how the incubation time affected cellular viability in the PDT groups. Nanoparticle concentrations of 5, 10, 25, 50, and 100 $\mu\text{g/ml}$ were chosen for PDT applications and named as PDT (nanoparticle concentration). Dual laser application was determined as a single dose and the material is specified in the methods section. According to the results of the viability analysis

using the 4h incubation time, the dual laser group increased the cellular viability compared to the control. Cellular viability was 95.16% and 94.85% in the PDT5 and PDT10 groups compared to the control. In the PDT 25, PDT50 and PDT100 groups, the viability decreased as the nanoparticle concentration increased. This clearly indicates increased cell damage as the concentration increases, due to the constant laser dose, as expected in the PDT mechanism. According to statistical analysis, all groups were not statistically significant. Likewise, in the groups using the 24h incubation time, the PDT25, PDT50, and PDT100 groups showed increased cellular death with increasing concentration. The viability of PC3 cells in PDT5 and PDT10 groups using 24h incubation was determined as 75.02% and 62.02% compared to the control. The decrease in cell viability in PDT groups applied with nanoparticles at 50 and 100 $\mu\text{g/ml}$ concentrations on PC3 showed the highest mortality with 40.44% and 25.14%. When the data are analyzed statistically, PDT5, PDT10, PDT25, PDT50, and PDT100 groups showed statistically significant results. When the different incubation times were compared in the PDT groups, the 24h incubation time was optimum for PDT effectiveness. In addition, when the PDT groups with nanoparticles at the same concentration were compared, the toxicity values of the 24h incubation times were higher. This proves that PDT is more effective in 24h nanoparticle incubation. The reason for this can be interpreted as more nanoparticles are taken into the cell at the end of 24h.

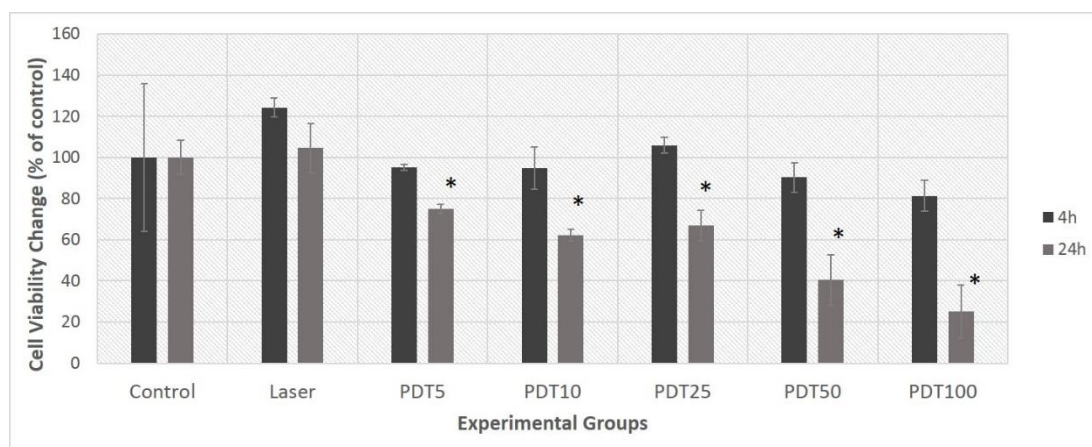


Figure 3.3.1c: Cell viability of only dual laser light, 5, 10, 25, 50, and 100 $\mu\text{g/mL}$ MSN-Ce6@PPI-ICG (%5) nanoparticles with dual-laser application after the 4h and 24h incubation time on PC3 cells. Statistically significant results are represented with * ($P < 0.05$).

Ji et al. observed cell viability reduction similar to our study by loading Ce6 and ICG into albumin nanoparticles. The phototoxicity they create is triggered by PDT and PTT

modulations. They achieved maximum phototoxicity in the group loaded with 1.25 $\mu\text{g/ml}$ Ce6 and 5 $\mu\text{g/ml}$ ICG. In our study, similar results were obtained by using 2.4 $\mu\text{g/ml}$ Ce6 and 1.8 $\mu\text{g/ml}$ ICG, and only the efficiency of the PDT pathways was increased. In addition, in their study, they observed that ICG and Ce6 quench each other. In our study, it has been proven that Ce6 and ICG in silica nanoparticles do not affect each other negatively. For this reason, we argue that our study yields more effective results in much easier ways [81].

Phototoxicity of MSN-Ce6@PPI Nanoparticles in L929

Anticancer PDT applications were also examined on healthy L929 cells to determine the side effects that may occur on the healthy tissue around the diseased tissue during anticancer PDT applications. The dual laser was applied to L929 cells with nanoparticles at the determined concentrations of 25, 50, and 100 $\mu\text{g/ml}$, and viability analyzes were carried out immediately after the application (0h) and 24h after the application (24h) to see the long-term effect (Figure 3.3.1d). According to the examinations made immediately after the application (0h), increased cell viability was decreasing with increasing nanoparticle concentration. Dual laser light did not show any toxic effect compared to control alone. As expected, PDT application caused damage to healthy cells as the concentration increased at the fixed laser dose. According to the statistical analysis results, all PDT groups showed statistically significant cell viability decreases. However, when the results after 24 hours of the application were examined, the viability of all PDT groups increased. Immediately after the application, the cellular viability in the PDT100 group was 53.91%, while it was 56.36% after 24 hours of the application. The increase in cell viability was higher in other PDT groups than in the PDT100 group. According to statistical analysis, PDT50 and PDT100 groups showed statistically significant results. This is an indication that PDT application can cause damage to healthy cells, but cells begin to be repaired within 24 h after treatment. It has been explained that nanoparticle-mediated PDT can increase cell proliferation by correct optimization of the size, incubation time, surface coating, morphology, and light parameters used of nanoparticles [82]. The results obtained after PDT application in our study also support this argument. It has also been reported that MSN-Ce6@PPI-ICG nanoparticles have selectivity for cancer cells as well as normal healthy cells [79]. It has been proven that

PDT application is specific to PC3 cancer cells, with the death rate being higher in cancer cells than in healthy L929 cells.

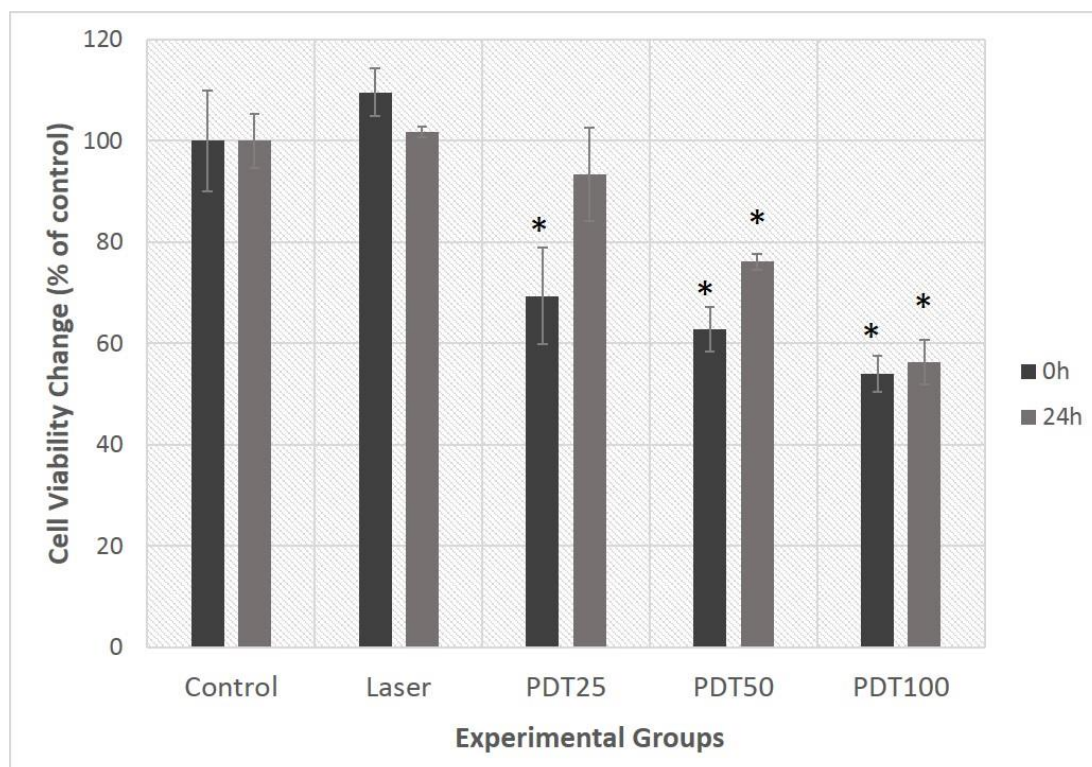


Figure 3.3.1d: Cell viability of only dual laser, 25, 50, and 100 $\mu\text{g}/\text{mL}$ MSN-Ce6@PPI-ICG (%5) nanoparticles with dual laser light at immediately after applications and 24h after the applications on L929 cells. Statistically significant results are represented with * ($P < 0.05$).

Photo/toxicity of Free Ce6 and ICG in PC3 Cells

To see the role of nanoparticles in PDT, groups were formed in which the free ICG and Ce6 photosensitizers loaded into MSN-Ce6@PPI-ICG nanoparticles were applied alone or in combination with the dual laser system (Figure 3.3.1e). By examining the viability analysis results, nanoparticle concentrations of 25, 50, 100 $\mu\text{g}/\text{mL}$ were determined and the amount of Ce6-ICG loaded on them was calculated (for 25 $\mu\text{g}/\text{mL}$ nanoparticle: 0.6 $\mu\text{g}/\text{mL}$ Ce6 and 0.45 $\mu\text{g}/\text{mL}$ ICG, for 50 $\mu\text{g}/\text{mL}$ nanoparticle: 1.2 $\mu\text{g}/\text{mL}$ Ce6 and 0.9 $\mu\text{g}/\text{mL}$ ICG, for 100 $\mu\text{g}/\text{mL}$ nanoparticle: 2.4 $\mu\text{g}/\text{mL}$ Ce6 and 1.8 $\mu\text{g}/\text{mL}$ ICG). The same concentrations were used in free form in applications. When the results were examined, the cell viability of the groups in which Ce6 photosensitizer was applied alone or in combination with the dual laser system was decreased at all concentrations compared to the control. In other words, Ce6 alone and together with

the dual laser system caused damage to PC3 cancer cells. However, statistical analysis results proved that these cell viability reductions were not statistically significant.

Later, when ICG photosensitizer was applied alone and together with the dual laser system, ICG groups except for L+ICG(NP(25)) caused a decrease in cellular viability. The drug concentrations decreased cell viability more than the groups using the dual laser system alone. According to the statistical analysis results, ICG(NP25), ICG(NP50), ICG(NP100), L+ICG(NP50), and L+ICG(NP100) groups showed a statistically significant decrease in cellular viability.

Then, due to the coexistence of ICG and Ce6 photosensitizers in nanoparticles, applications were repeated by mixing free ICG and Ce6 photosensitizer at the determined concentration to examine the effect of nanoparticles in these groups, without a dual laser system and by excitation with the dual laser system. According to the viability analysis results, a decrease and/or increase in cell viability was observed compared to the control. However, these changes were not found to be significant when analyzed statistically except [Ce6+ICG(NP100)]+L. Although this group showed significant reductions, the phototoxicity of photosensitizers was higher when in the nanoparticle. This result has shown us that ICG and Ce6 photosensitizers have a toxic effect at only higher concentrations on PC3 cancer cells when mixed in the same environment. When ICG and Ce6 were found inside of the nanoparticle structure, viability was 25.14% in this group. But their free forms showed 80.51% viability. So, nanoparticles showed higher toxicity when compared to free groups.

The light-free applications of ICG and Ce6 on cancer cells were to see the importance of MSN and to examine the effect of the concentrations used in free form. Mortality rates in the free states of Ce6 and ICG in the created groups are lower than their state in nanoparticles. In other words, the MSN structure has increased the efficiency of Ce6 and ICG. We explained this situation, that the nanoparticle structure protects the photosensitizers while they are transported into the cell and allows the PDT mechanism to work by activating only inside the cell. In conclusion, we argued that nanoparticles increase the uptake of photosensitizers into cells. These results also

overlapped with cellular uptake results. At increasing concentrations, the uptake of nanoparticles and thus photosensitizers is enhanced.

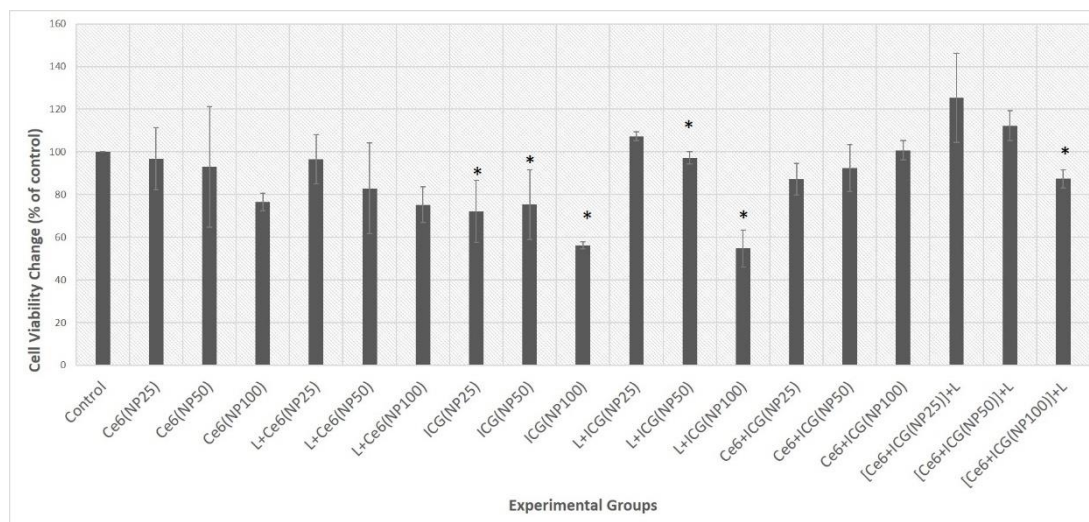


Figure 3.3.1e: Cell viability with free Ce6 and ICG photosensitizers that are found inside of the 25, 50 and 100 $\mu\text{g}/\text{mL}$ MSN-Ce6@PPI-ICG nanoparticles and their PDT applications with dual laser light on PC3 cells (Free photosensitizer concentrations; for 25 $\mu\text{g}/\text{mL}$ nanoparticle: 0.6 $\mu\text{g}/\text{mL}$ Ce6 and 0.45 $\mu\text{g}/\text{mL}$ ICG, for 50 $\mu\text{g}/\text{mL}$ nanoparticle: 1.2 $\mu\text{g}/\text{mL}$ Ce6 and 0.9 $\mu\text{g}/\text{mL}$ ICG, for 100 $\mu\text{g}/\text{mL}$ nanoparticle: 2.4 $\mu\text{g}/\text{mL}$ Ce6 and 1.8 $\mu\text{g}/\text{mL}$ ICG and dual laser parameters; for 655nm diode laser; 300mW power, 120J/cm² energy density, for 808nm diode laser; 600mW power, 240J/cm² energy density, 706s application time). Statistically significant results are represented with * (P<0.05).

3.3.2 Cellular Uptake of MSN-Ce6@PPI-ICG Nanoparticles in PC3 Cells

In order to determine whether MSN-Ce6@PPI-ICG nanoparticles were taken up into the cells at 25, 50, and 100 $\mu\text{g}/\text{mL}$ concentrations, absorbed wavelength values of Ce6 and ICG showing maximum absorbance were used in Triton-100X application (Figure 3.3.2). We expected to see high absorbance values at specific wavelengths for Ce6 and ICG in cell solutions that were lysed as a result of the Triton-100X application. In the absorbance spectrum obtained after incubation of the determined concentrations with the PC3 cells, specific wavelengths of free Ce6 and ICG in the nanoparticles taken into the cell and showing maximum absorbance values were also observed. This indicates that the nanoparticles successfully penetrate the cell at all concentrations. The increase in absorbance values with the increase of nanoparticle concentration shows that as the concentration increases, the penetration of nanoparticles into the cell is greater. This

is more clearly observed at the specific wavelength of the ICG in the absorbance spectrum analysis. These results confirmed the data of decreased cellular viability with increasing nanoparticle concentration.

In the PDT mechanism, the uptake of PS into the cell and its localization in the cell are very important. Because it is known that the half-life of ROS formed as a result of PDT is quite short, and the diffusion distance is limited and short. In order for the formed ROS to cause effective damage, PS must be taken into the cell [87]. In our study, it was shown that the obtained phototoxicity was successfully achieved with PDT. In the PDT100 group with the highest amount of nanoparticles taken into the cell, the more dead cells were seen in the Acridine Orange/Propidium Iodide staining, and the highest PC3 death was observed in the MTT viability analysis in the same group.

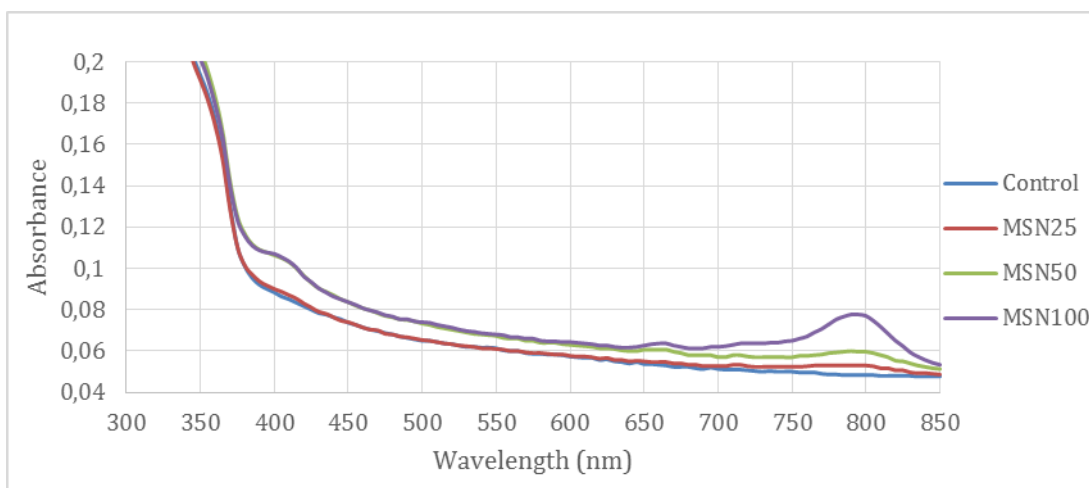


Figure 3.3.2: Absorbance Spektrum of 25, 50 and 100 $\mu\text{g}/\text{mL}$ MSN-Ce6@PPI-ICG nanoparticles in Triton-100X and PC3 cell solutions after 24h incubation.

3.3.3 Acridine Orange/Propidium Iodide Staining

The results of Acridine Orange/Propidium Iodide staining were applied to the 25, 50, and 100 $\mu\text{g}/\text{mL}$ nanoparticle concentrations and their PDT groups on PC3 cells then results were obtained by fluorescence microscopy (Figure 3.3.3). Looking at the images, dead red cells are seen more intensely in MSN100, PDT50, and PDT100 groups. In groups with dense live cells, such as control, cells are generally observed in green. When the images are examined, the dual laser, 25 and 50 $\mu\text{g}/\text{mL}$ nanoparticle

groups are mostly similar to the control group in terms of living cells. Dual laser, 25 and 50 $\mu\text{g}/\text{mL}$ nanoparticle applications alone did not cause cell death. These results were found to be compatible with the viability analysis results. It is understood that cellular death increased in MSN100, PDT25, PDT50, and PDT100 groups, in which the density of red dead cells started to increase. The MSN100 group produced 26.66% cellular death as found in viability assays on the PC3 cancer line. The increased red cell density in the PDT25, PDT50, and PDT100 groups confirm the cellular death rates of 33.12%, 59.56%, and 74.86%, respectively, seen in the viability analysis. In general, the results of acridine orange propidium iodide staining, which allows seeing dead and living cells, were found to be compatible with the results of other analysis methods in which the anticancer PDT efficacy was proven.

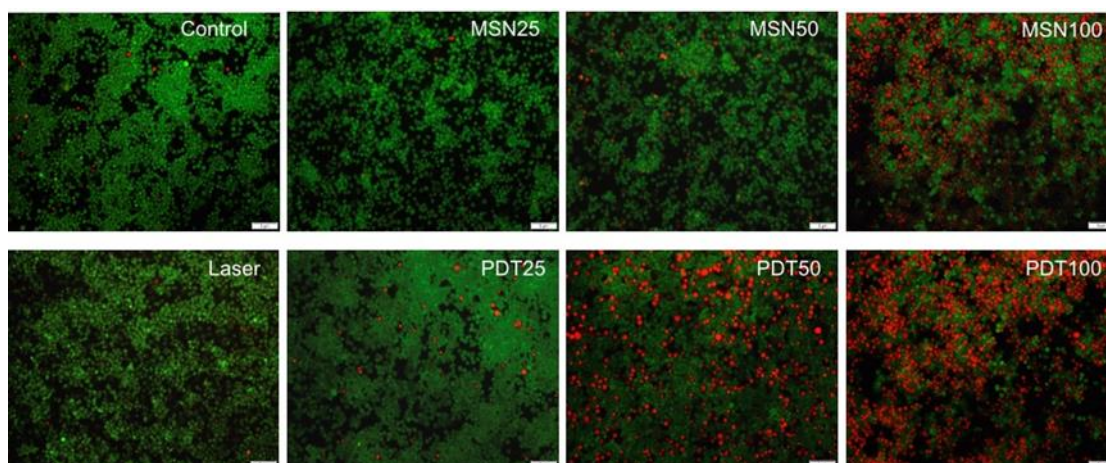


Figure 3.3.3: Acridine orange (live cell, green) / Propidium Iodide (dead cell, red) images of dual laser, 25, 50 and 100 $\mu\text{g}/\text{mL}$ MSN-Ce6@PPI-ICG nanoparticles and their PDT applications with dual laser application on PC-3 cells.

3.3.4 DAPI Staining

DAPI staining was a nuclear visualization test of PC-3 cells as a result of treatments. Fluorescence images obtained as a result of staining are presented (Figure 3.3.4). Since it was desired to monitor the cell nucleus damage of PDT activity, the control group and all PDT groups were stained. When the images were examined, the nuclei of the cells showed changes in the PDT groups compared to the control group. A denser, non-scattering, large and mononuclear core structure was observed in the control group. These features are characteristics of a healthy cell nucleus. However, when PDT groups are examined, deterioration in the core structure, leakage, doubled and

small core structure are observed. Distortions are exemplified on the image by orange arrows. These features are those of the cell nucleus entering the apoptosis pathway and are seen in PDT groups. Also, the incidence of disrupted core structure increased with increasing nanoparticle concentration. In the PDT100 group, where maximum cellular death was observed, these defective nuclear structures were observed quite frequently. In addition to mitochondrial-related cellular destructions in the PDT mechanism, it is known that oxidative damage is created in DNA when the excess ROS formed and damaged the redox system of the cell [87]. This can be seen in DAPI staining in the form of deterioration of the structure of the core or core leakage. With the DAPI images of the PDT groups that we created, it was confirmed that this way they cause irreversible cell nuclei and DNA damages in the cell.

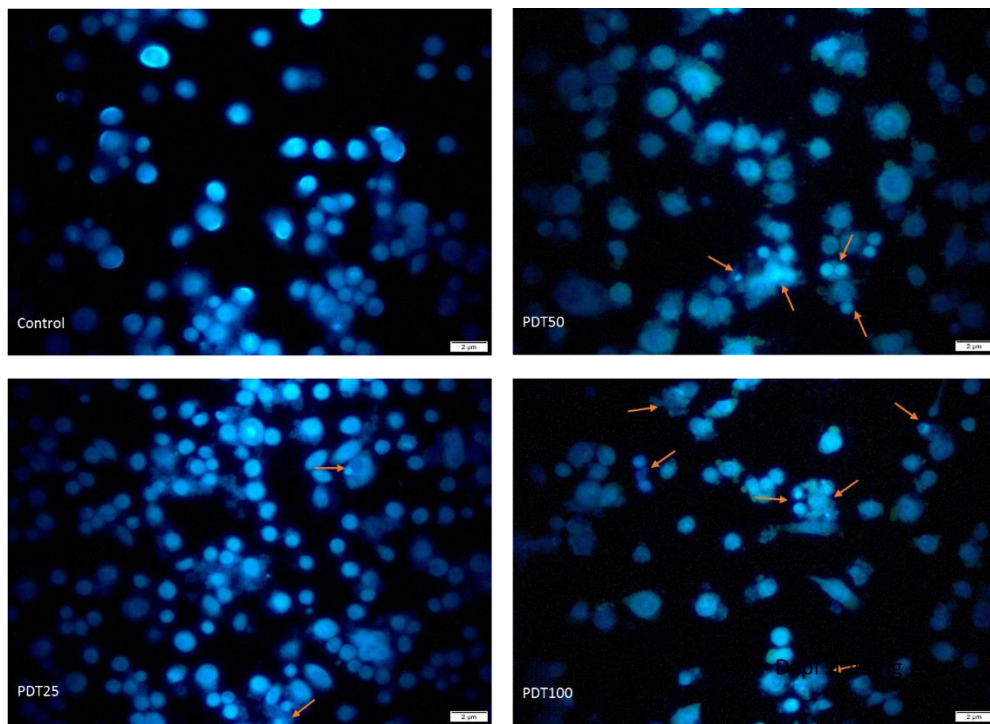


Figure 3.3.4: DAPI Staining images of PDT groups with 25, 50 and 100 $\mu\text{g}/\text{mL}$ MSN-Ce6@PPI-ICG nanoparticles and dual optic laser light application on PC-3 cells.

3.4 Mechanistic Analysis

3.4.1 Reactive Oxygen Species Measurements in PC3 Cells after the PDT Applications

It is known that cell death occurs as a result of ROS-mediated cellular damage in the molecular mechanism of PDT. A decrease in cellular viability is expected in direct relationship to the amount of ROS formation. Because of this important role of ROS in the PDT mechanism, dual laser light, 25, 50, and 100 $\mu\text{g/ml}$ nanoparticle concentrations and their PDT groups were tested with a DCFH-DA probe (Figure 3.4.1). Measurements were taken immediately after the application, as ROS formation starts immediately after the specific application to the cell and affects the cells. When the results were examined, more ROS formation was observed in all groups compared to the control group. It is known that a ROS formation originating from light and/or nanoparticles occurs in laser and PDT groups with dual laser application. In nanoparticle groups, it is thought that ROS is formed as a result of stimulation of cancer cells by an external factor such as nanoparticles. Because of this idea, MSN25, MSN50, and MSN100 groups showed higher ROS formation when compared to control. In the PDT25 group, where the nanoparticle concentration was the lowest, therefore, the ROS formation was minimally increased. There was a 22.13% increase in ROS in the PDT50 group compared to the control. It was observed that the PDT100 group with the lowest cellular viability produced more ROS than the other groups, and there was an increase of 89.71% compared to the control. It has been shown that the toxic effect in the PDT mechanism is mostly directed by ROS, with the results of decreasing cellular viability with increasing ROS formation. According to statistical

analysis, only the PDT100 group showed statistically significant results when compared to the control group.

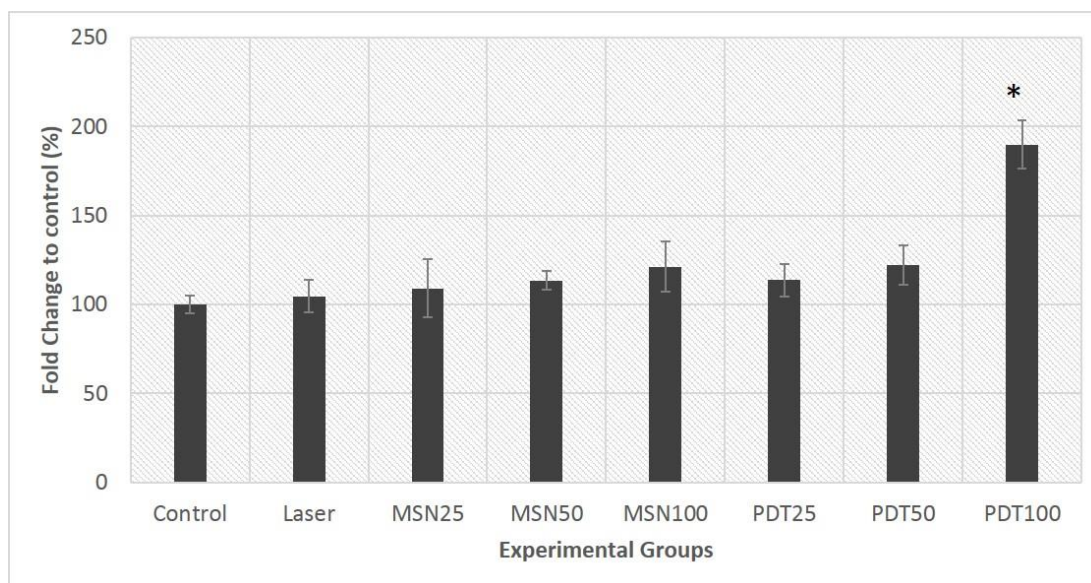


Figure 3.4.1: Reactive Oxygen Species formation of dual laser light, 25, 50, and 100 $\mu\text{g/mL}$ nanoparticles and their PDT groups with dual laser on PC3 cells. Statistically significant results are represented with * ($P < 0.05$).

Mitochondria-targeted and ROS-mediated therapy methods are widely used in cancer treatment. Because ROS formed in ROS-mediated treatments cuts the energy supply of cancer cells by affecting mitochondria and triggers mitochondrial dependent cell death. In addition, the generated ROS must exceed a certain level in order to provide toxicity. In this way, the increase in ROS in the PDT mechanism increases the toxicity [88]. Therefore, increases in ROS production were observed in all groups with light and nanoparticle application. As seen in AO/PI images, ROS production increased in PDT and MSN groups with dense red dead cells. The high frequency of nuclear disruption in the PDT100 group in DAPI images proved that the oxidative stress was caused by ROS. According to Topaloglu et al. PC3 reduced cell viability by 89% as a result of the interaction of 655nm red light with TBO in prostate cancer cells. They supported that the mechanism was ROS dependent by ROS measurements [83]. The fact that the maximum effect was observed in our study at 100 $\mu\text{g/ml}$ nanoparticle concentration confirms this.

3.4.2 Mitochondrial Membrane Potential of PC3 Cells after PDT Applications

JC-1 is a fluorogenic probe and forms red fluorescent aggregates in dimer form when the mitochondrial membrane potential is high. It fluoresces green in monomer form when the mitochondrial membrane potential is low. Therefore, the red/green fluorescence ratio indicates changes in mitochondrial membrane potential. In cells entering the apoptosis pathway, the mitochondrial membrane potential value is expected to be low, since the mitochondrial membrane cannot be polarized. In direct relation to this, the red/green ratio is expected to be below. The results of MMP analysis performed on dual laser, 25, 50, and 100 $\mu\text{g/mL}$ nanoparticles, and their PDT groups are presented below (Figure 3.4.2a). Dual laser light showed similar MMP change when compared to control. Decreased cellular viability with increasing nanoparticle concentration in the viability analysis results in PDT groups gave decreased MMP results here. In the PDT25, PDT50, and PDT100 groups in which dead cells increased, the green/red ratio decreased as a result of the decrease in MMP. These results were expected in the PDT groups. Also, this situation coincided with the viability analysis results. It was observed that MMP increased in groups where laser and nanoparticles were applied alone. In this case, it is thought that there is an increase in MMP, which indicates that the cell goes to the survival state as a result of the stress in the cells and that the energy production increases in the cell. This resulted in the MMP increasing. Although the results were not statistically significant, the results were compatible with the viability analysis.

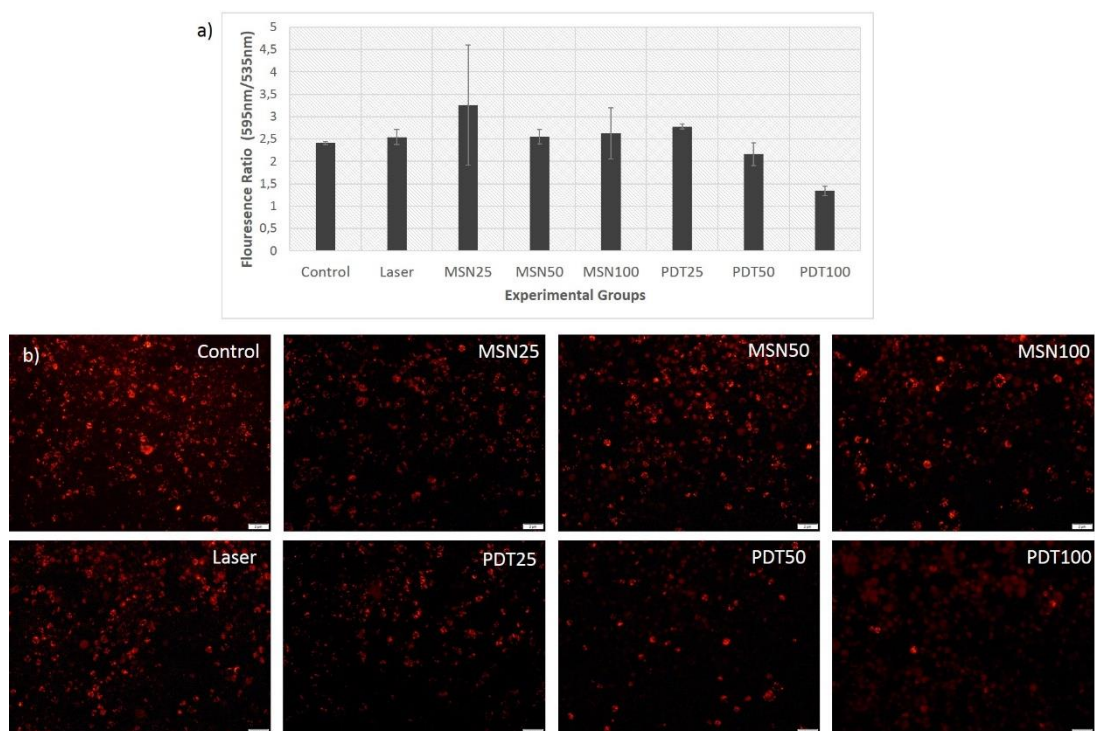


Figure 3.4.2: JC-1 Mitochondrial Membrane Potential Assay Measurements a) Fluorescence values of dual laser light, 25, 50 and 100 $\mu\text{g/mL}$ MSN-Ce6@PPI-ICG nanoparticles and their PDT applications on PC3 cells b) JC-1 Aggregates images of living cells in dual laser light, 25, 50 and 100 $\mu\text{g/mL}$ MSN-Ce6@PPI-ICG nanoparticles and their PDT applications on PC3 cells. Statistically significant results are represented with * ($P < 0.05$).

In addition, we observed red-luminescent JC-1 aggregates observed in polarizable cells in images taken by fluorescence microscopy (Figure 3.4.2b). In the control, it was observed that healthy cells could be polarized, resulting in the formation of JC-1 aggregates as red dots. However, the amount of these aggregates decreases towards groups with increased cellular death. These images were also compatible with red/green MMP fluorescence measurements. The lowest mitochondrial membrane potential in the PDT groups is seen in the images and fluorescence measurements. These results were a different perspective proving that the PDT mechanism works successfully in PC-3 cells.

In short, it is known that the mechanism of PDT is the absorption of light by the mitochondria and that the mitochondrial membrane changes in this way. With the signals released to the mitochondria by different organelles by chemical means, there is a decrease in MMP due to non-polarization. Thus, ROS production is promoted. In other words, cell death in PDT begins with the depolarization of MMP [88]. In dead cells, ie groups in which PDT is active, MMP is expected to be low because this change

is not polarized [84]. In our study, MMP changes were decreased in the groups in which PDT was effective. In addition to the numerical data, JC1 cluster images also explain the reduction in red clusters in the PDT groups.

3.4.3 Nitric Oxide Releasing in PC3 Cells after the PDT Applications

NO is a molecule released from the mitochondria after light application in the PDT mechanism and can cause toxicity. The realization of NO production in the PDT mechanism and the toxic effect is shown as another proof that the PDT mechanism occurs. Determining the amount of NO, therefore, indicates an effective PDT application. Nitrite amounts were calculated using Griess reagent after nanoparticle and/or dual laser applications to PC-3 cancer cells (Figure 3.4.3). The amount of nitrite has a directly proportional relationship with the NO released. The results of NO release as a result of PDT applications of nanoparticles alone or together with a dual laser system at 25, 50, and 100 $\mu\text{g}/\text{mL}$ concentrations are given. Dual laser application alone showed some NO release in PC3 cells compared to the control group. In the groups where nanoparticles were applied alone, NO release was decreased at 25 and 50 $\mu\text{g}/\text{ml}$ concentrations compared to the control, while 100 $\mu\text{g}/\text{ml}$ nanoparticles increased NO release. These results supported the low toxicity of 25 and 50 $\mu\text{g}/\text{ml}$ nanoparticles compared to 100 $\mu\text{g}/\text{mL}$ nanoparticles. The reason for the toxicity seen in the MSN100 group may be due to the higher formation of toxic products such as NO and ROS in this group. In the PDT groups, on the other hand, increased NO release was observed with increasing nanoparticle concentration compared to the control. NO release in these groups was higher than the other groups. This is another proof that the PDT mechanism occurs successfully in PDT groups. Even in the groups with low nanoparticle concentration, NO release results showed that the PDT mechanism worked. In addition, as the concentration increases, the increase in NO release coincides with the viability analysis results. This has been proven with the highest NO release in the PDT groups with the lowest cellular viability. Although there were no statistically significant differences when the results were analyzed, the NO release results were in agreement with other viability analyses.

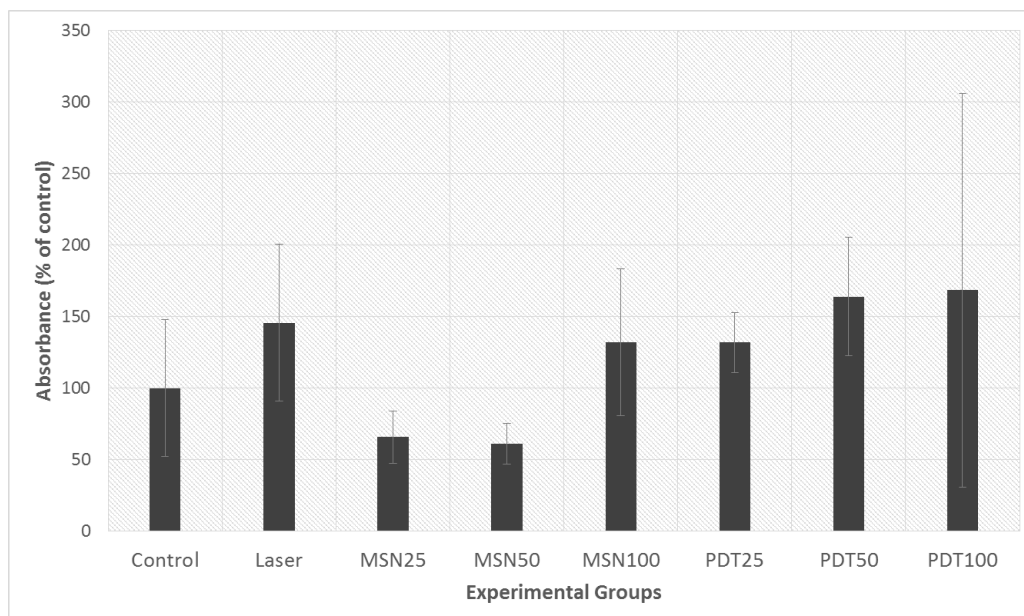


Figure 3.4.3: Nitrite amounts of dual laser light, 25, 50 and 100 $\mu\text{g}/\text{mL}$ MSN-Ce6@PPI-ICG nanoparticles and their PDT applications with dual laser on PC-3 cells. Statistically significant results are represented with * ($P < 0.05$).

In the PDT mechanism, NO is released by the mitochondria as a result of the absorption of light. NO release also creates a toxic effect like ROS and the toxicity increases with NO and ROS [85]. In addition, the amount of NO release has been found to cause different effects in cancer cells. It has been shown that low level NO release creates a more aggressive tumor population and triggers the formation of resistant tumors. In the same study, it was proven that high NO release creates cell growth arrest [89]. Therefore, we expected high NO release in the groups with the maximum decrease in viability in PDT. As we expected in the results, NO release increased in groups with high PDT toxicity. In addition, an increase in NO release was observed in groups with increased ROS production. In addition, lower NO release in MSN25 and MSN50 groups, where death is seen at low levels, is also in line with the above-mentioned logic. We have shown that the created nanoparticle and laser system constitutes a successful PDT mechanism.

3.5 Temperature Measurements during Dual Laser Optical System Applications

Since there is energy transfer to the target area during the dual laser application, the temperature increase that may occur in the target was measured with a thermal camera.

In addition, there is a possibility that nanoparticles can create a thermal effect when applied with the dual system. For this reason, temperature analysis was performed with a thermal camera to the groups in which dual laser was applied (Figure 3.5). When the temperature measurements were taken at certain intervals during laser application are examined; dual laser application alone showed lower temperature values than PDT groups. When the PDT groups were examined, the temperature values formed in the environment increased as the nanoparticle concentration increased. This indicates that the nanoparticles increase the interaction in the environment with the dual laser, compared to the dual laser application alone. Considering the temperature differences at the beginning and end of the application in the groups, the temperature differences in the dual laser light, PDT25, PDT50, and PDT100 groups were 1.6, 0.5, 0.6, and 0.8, respectively. The highest temperature difference in the laser group may be due to the coldness of the application environment since it is the first applied group. There is an energy transfer due to the energy transferred during the application of light. In addition, a temperature increase created by nanoparticle application may also be in question in this study. Especially the temperature increase created by the Ce6 and ICG photosensitizers used can create a photothermal effect on the cells. It is known that ICG creates an increase in temperature in photothermal studies. For this reason, the temperature rise was measured in the study. But the results vary between 0 and 2 °C. Moreover, these temperature differences are too low to cause any thermal cellular damage in a healthy or cancerous cell. These results also suggest that the anticancer activity is mediated by PDT via photochemical interaction mechanisms, not thermal.

In the study of Ji et al., it was determined that ICG and Ce6 loaded albumin nanoparticles caused a temperature increase of about 12°C and death effect was created with PTT. It is known that ICG photosensitizer causes thermal effect [86]. It is quite natural to see this thermal effect due to the high amount of ICG loaded in their study. This thermal increase has the capacity to cause thermal damage to the healthy surrounding tissue. However, since the amount of ICG loaded in our study was at low concentrations, the temperature increase was low. This shows that the thermal effect created on the surrounding tissue will be minimal [81].

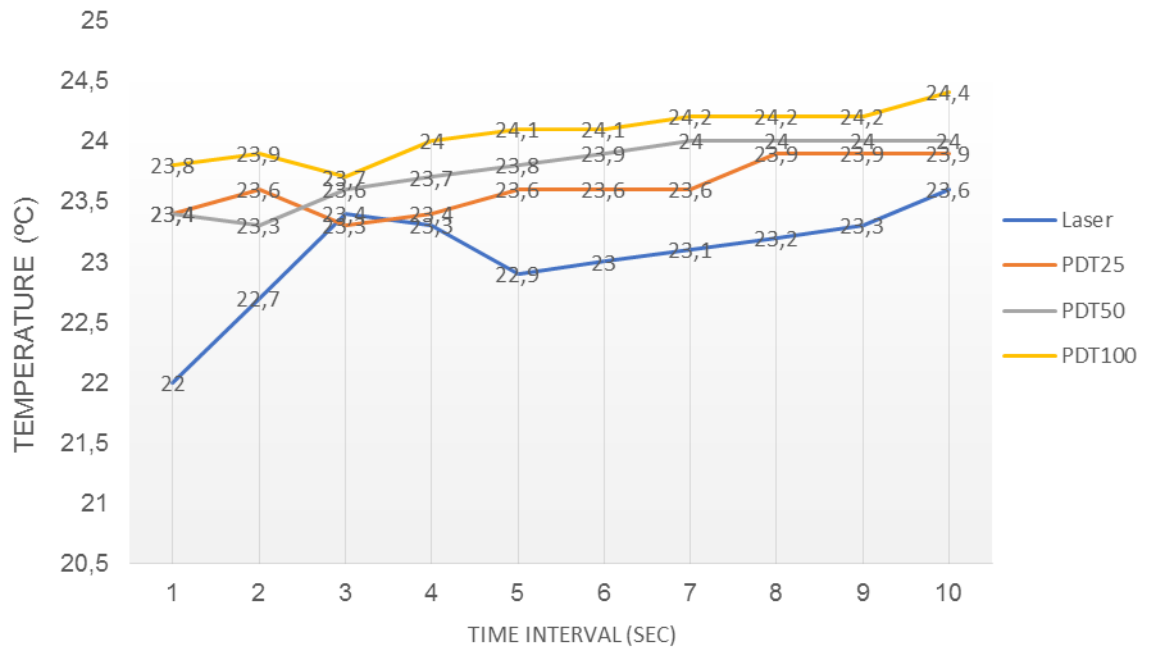


Figure 3.5: Temperature Measurements with thermal camera for dual laser light, PDT25, PDT50, and PDT100 groups.

Chapter 4

Conclusion

PDT is a light therapy method used in the treatment of cancer and infectious diseases. The mechanism of PDT begins with photosensitive agents converting energy from light. This energy triggers the production of mitochondria-targeted ROS through biological and chemical changes in the diseased tissue. The resulting ROS causes cellular death in the diseased cell by affecting different cell components and their functioning. The amount of ROS formed and its location in the cell determines the effect of PDT. This shows the importance of the location of photosensitive agents in the cell. For this reason, nanoparticle technology is quite capable of increasing the efficiency of photosensitizers in PDT. In this study, we created MSN-Ce6@PPI-ICG nanoparticles by loading Ce6 and ICG photosensitizers into MSN nanoparticles. To activate this dual nanoparticle structure, we designed a dual laser system using 655nm and 808nm laser light. We used a dual laser optics system and dual nanoparticles in our PDT applications. We observed maximum cellular death in PC3 cells using low concentrations of photosensitizers and light with nanoparticle structure. In addition, with the nanoparticle structure, the specific uptake of photosensitizers into cancer cells and their ROS production capacity were increased. The efficiency of PDT was increased by using two different photosensitizers in the same nanoparticle. The claimed PDT efficacy was proven by viability analysis, acridine orange/propidium iodide, DAPI, ROS, MMP, and NO measurements. In addition, with the temperature measurements, it was shown that the effects seen only with the PDT mechanism were

created without any thermal damage. This study will be very useful in reducing photosensitizer and light concentrations for *in vivo* and clinical studies.

References

- [1] Raab, O. Uber die wirkung fluorescirender stoffe auf infusorien. *Z. biol.* 1900: 39: 524-546.
- [2] Jesionek, A., & von Tappenier, H. Zur behandlung der hautcarcinomit mit fluorescierenden stoffen. *Muench Med Wochneshr* 1903: 47: 2042.
- [3] Henderson, B. W., & Dougherty, T. J. How does photodynamic therapy work?. *Photochemistry and photobiology* 1992: 55(1): 145-157.
- [4] Photochemistry and photobiology, 55(1), 145-157. Perry, R. R., Smith, P. D., Evans, S. & Pass, H. I. Intravenous vs intraperitoneal sensitizer: implications for intraperitoneal photodynamic therapy. *Photochem. Photobiol.* 1991: 53: 335–340.
- [5] Li, X., Lovell, J. F., Yoon, J., & Chen, X. Clinical development and potential of photothermal and photodynamic therapies for cancer. *Nature Reviews Clinical Oncology* 2020: 17(11): 657-674.
- [6] Xu, J., Gao, J., & Wei, Q. Combination of photodynamic therapy with radiotherapy for cancer treatment. *Journal of Nanomaterials*, 2016.
- [7] Sibata, C. H., Colussi, V. C., Oleinick, N. L., & Kinsella, T. J. Photodynamic therapy: a new concept in medical treatment. *Brazilian Journal of Medical and Biological Research* 2000: 33(8): 869-880.
- [8] Chilakamarthi, U., & Giribabu, L. Photodynamic therapy: past, present and future. *The Chemical Record* 2017: 17(8): 775-802.

- [9] Oniszczyk, A., Wojtunik-Kulesza, K. A., Oniszczyk, T., & Kasprzak, K. The potential of photodynamic therapy (PDT)—Experimental investigations and clinical use. *Biomedicine & Pharmacotherapy* 2016; 83: 912-929.
- [10] Castano, A. P., Demidova, T. N., & Hamblin, M. R. Mechanisms in photodynamic therapy: part one—photosensitizers, photochemistry and cellular localization. *Photodiagnosis and photodynamic therapy* 2004; 1(4): 279-293.
- [11] C. Tanielian, R. Mechin, R. Seghrouchni, C. Schweitzer, *Photochem. Photobiol.* 2000; 71: 12–19.
- [12] Laustriat, G. Molecular mechanisms of photosensitization. *Biochimie* 1986; 68(6): 771-778.
- [13] Oszejca, M., Brindell, M., Orzeł, Ł., Dąbrowski, J. M., Śpiwak, K., Łabuz, P., ... & Stochel, G. Mechanistic studies on versatile metal-assisted hydrogen peroxide activation processes for biomedical and environmental incentives. *Coordination Chemistry Reviews* 2016; 327: 143-165.
- [14] Vakrat-Haglili, Y., Weiner, L., Brumfeld, V., Brandis, A., Salomon, Y., McIlroy, B., ... & Scherz, A. The microenvironment effect on the generation of reactive oxygen species by Pd–bacteriopheophorbide. *Journal of the American Chemical Society* 2005; 127(17): 6487-6497.
- [15] Macdonald, I. J., & Dougherty, T. J. Basic principles of photodynamic therapy. *Journal of Porphyrins and Phthalocyanines* 2001; 5(02): 105-129.
- [16] Kwiatkowski, S., Knap, B., Przystupski, D., Saczko, J., Kędzierska, E., Knap-Czop, K., ... & Kulbacka, J. Photodynamic therapy—mechanisms, photosensitizers and combinations. *Biomedicine & Pharmacotherapy* 2018; 106: 1098-1107.
- [17] Jin, F., Di Liu, X. X., Ji, J., & Du, Y. Nanomaterials-Based Photodynamic Therapy with Combined Treatment Improves Antitumor Efficacy Through Boosting Immunogenic Cell Death. *International Journal of Nanomedicine* 2021; 16: 4693.

- [18] Star, W. M. Light delivery and light dosimetry for photodynamic therapy. *Lasers in Medical Science* 1990: 5(2): 107-113.
- [19] Svaasand LO. Optical dosimetry for direct and interstitial photoradiation therapy of malignant tumors. *Prog Clin Biol Res* 1984;170:91—114.
- [20] Chiniforush, N., Pourhajibagher, M., Parker, S., Benedicenti, S., Shahabi, S., & Bahador, A. The effect of sublethal photodynamic therapy on the expression of Enterococcal surface protein (esp) encoding gene in *Enterococcus faecalis*: Quantitative real-time PCR assessment. *Photodiagnosis and photodynamic therapy* 2018: 24: 311-317.
- [21] Brancalion, L., & Moseley, H. Laser and non-laser light sources for photodynamic therapy. *Lasers in medical science* 2002: 17(3): 173-186
- [22] Davanzo, N. N., Pellosi, D. S., Franchi, L. P., & Tedesco, A. C. Light source is critical to induce glioblastoma cell death by photodynamic therapy using chloroaluminiumphthalocyanine albumin-based nanoparticles. *Photodiagnosis and photodynamic therapy* 2017: 19: 181-183.
- [23] Chiniforush, N., Pourhajibagher, M., Parker, S., Benedicenti, S., Bahador, A., Sălăgean, T., & Bordea, I. R. The Effect of Antimicrobial Photodynamic Therapy Using Chlorophyllin–Phycocyanin Mixture on *Enterococcus faecalis*: The Influence of Different Light Sources. *Applied Sciences* 2020: 10(12): 4290.
- [24] Allison RR, Downie GH, Cuenca R, Hu XH, Childs CJ, Sibata CH. Photosensitizers in clinical PDT. *Photodiagnosis Photodyn Ther* 2004;1: 27-42.
- [25] Allison, R. R., & Moghissi, K. Photodynamic therapy (PDT): PDT mechanisms. *Clinical endoscopy* 2013: 46(1): 24.
- [26] Abrahamse, H., & Hamblin, M. R. New photosensitizers for photodynamic therapy. *Biochemical Journal* 2016: 473(4): 347-364.
- [27] N. Topaloglu, M. Guney, N. Aysan, M. Gulsoy, S. Yuksel, The role of reactive oxygen species in the antibacterial photodynamic treatment: photoinactivation vs proliferation, *Lett. Appl. Microbiol.* 2016: 62(3): 230-236.

- [28] A.P. Castano, T.N. Demidova, M.R. Hamblin, Mechanisms in photodynamic therapy: Part three—Photosensitizer pharmacokinetics, biodistribution, tumor localization and modes of tumor destruction, *Photodiagn. Photodyn. Ther.* 2005: 91–106.
- [29] Sabino, C. P., Wainwright, M., Ribeiro, M. S., Sellera, F. P., Dos Anjos, C., da Silva Baptista, M., & Lincopan, N. Global priority multidrug-resistant pathogens do not resist photodynamic therapy. *Journal of Photochemistry and Photobiology B: Biology* 2020: 208: 111893.
- [30] M.B. Vrouenraets, G.W.M. Visser, G.B. Snow, G.A.M.S. van Dongen, Basic principles, applications in oncology and improved selectivity of photodynamic therapy, *Anticancer Res.* 23 (1B) 2003: 505–522
- [31] Dąbrowski, J. M. Reactive oxygen species in photodynamic therapy: mechanisms of their generation and potentiation. *Advances in Inorganic Chemistry* 2017: 70: 343-394.
- [32] Lange, C., Lehmann, C., Mahler, M., & Bednarski, P. J. Comparison of cellular death pathways after mTHPC-mediated photodynamic therapy (PDT) in five human cancer cell lines. *Cancers* 2019: 11(5): 702.
- [33] Mallidi, S.A.S.; Bulin, A.L.; Obaid, G.; Ichikawa, M.; Hasan, T. Beyond the Barriers of Light Penetration: Strategies, Perspectives and Possibilities for Photodynamic Therapy. *Theranostics* 2016: 6: 2458–2487
- [34] Kim, M. M., & Darafsheh, A. Light sources and dosimetry techniques for photodynamic therapy. *Photochemistry and photobiology* 2020: 96(2): 280-294.
- [35] Yi, G., Hong, S. H., Son, J., Yoo, J., Park, C., Choi, Y., & Koo, H. Recent advances in nanoparticle carriers for photodynamic therapy. *Quantitative imaging in medicine and surgery* 2018: 8(4): 433.
- [36] Sivasubramanian, M., Chuang, Y. C., & Lo, L. W. Evolution of nanoparticle-mediated photodynamic therapy: from superficial to deep-seated cancers. *Molecules* 2019: 24(3): 520.

- [37] Banfield, J. F., & Zhang, H. Nanoparticles in the environment. *Reviews in mineralogy and geochemistry* 2001: 44(1): 1-58
- [38] Fukuda Metal Foil and Powder Co. Ltd. [Internet]. China 2021 [cited by 10.08.2021]. Available from: <https://www.fukuda-kyoto.co.jp/en/technology/research/nanoparticles.html>
- [39] Lucky, S. S., Soo, K. C., & Zhang, Y. Nanoparticles in photodynamic therapy. *Chemical reviews* 2015 115(4): 1990-2042.
- [40] Yin, R., Agrawal, T., Khan, U., Gupta, G. K., Rai, V., Huang, Y. Y., & Hamblin, M. R. Antimicrobial photodynamic inactivation in nanomedicine: small light strides against bad bugs. *Nanomedicine* 2015:10(15): 2379-2404
- [41] Kateb B, Chiu K, Black KL et al. Nanoplatfoms for constructing new approaches to cancer treatment, imaging, and drug delivery: what should be the policy? *Neuroimage* 54(Suppl. 1), S106–S124 (2011).
- [42] Wang, C., Cheng, L., & Liu, Z. Upconversion nanoparticles for photodynamic therapy and other cancer therapeutics. *Theranostics* 2013: 3(5): 317.
- [43] Feng, Y., Wu, Y., Zuo, J., Tu, L., Que, I., Chang, Y., ... & Zhang, H. Assembly of upconversion nanophotosensitizer in vivo to achieve scatheless real-time imaging and selective photodynamic therapy. *Biomaterials* 2019: 201: 33-41.
- [44] Feng, Y., Wu, Y., Zuo, J., Tu, L., Que, I., Chang, Y., ... & Zhang, H. Assembly of upconversion nanophotosensitizer in vivo to achieve scatheless real-time imaging and selective photodynamic therapy. *Biomaterials* 2019: 201: 33-41.
- [45] Couleaud P, Morosini V, Frochot C, Richeter S, Raehm L, Durand JO. Silica-based nanoparticles for photodynamic therapy applications. *Nanoscale* : 2010, 2: 1083 – 1095.
- [46] Lu, J., Liong, M., Li, Z., Zink, J. I., & Tamanoi, F. Biocompatibility, biodistribution, and drug-delivery efficiency of mesoporous silica nanoparticles for cancer therapy in animals. *Small* 2010: 6(16): 1794-1805.

- [47] Huang, Y. Y., Sharma, S. K., Dai, T., Chung, H., Yaroslavsky, A., Garcia-Diaz, M., ... & Hamblin, M. R. Can nanotechnology potentiate photodynamic therapy?. *Nanotechnology reviews* 2012: 1(2): 111-146
- [48] Couleaud P, Morosini V, Frochot C, Richeter S, Raehm L, Durand JO. Silica-based nanoparticles for photodynamic therapy applications. *Nanoscale* . 2010, 2, 1083 – 1095.
- [49] Liu, J., Karaman, D. Ş., Zhang, J., Rosenholm, J. M., Guo, X., & Cai, K. NIR light-activated dual-modality cancer therapy mediated by photochemical internalization of porous nanocarriers with tethered lipid bilayers. *Journal of Materials Chemistry B* 2017: 5(42): 8289-8298.
- [50] Şen Karaman, D. (2016). Physicochemical characteristics of silica nanoparticles tailored for nanomedicine.
- [51] Bakay, E., Karaman, D. Ş., & Topaloğlu, N. (2019, October). The Effect of Different Concentrations of Mesoporous Silica Nanoparticles in Antibacterial Photodynamic Therapy. In 2019 Medical Technologies Congress (TIPTEKNO) (pp. 1-4). IEEE.
- [52] Auger, A., Samuel, J., Poncelet, O., & Raccurt, O. A comparative study of non-covalent encapsulation methods for organic dyes into silica nanoparticles. *Nanoscale research letters* 2011: 6(1): 1-12.
- [53] Amin, A., & Kaduskar, D. V. Comparative Study on Photodynamic Activation of Ortho-Toluidine Blue and Methylene Blue Loaded Mesoporous Silica Nanoparticles Against Resistant Microorganisms. *Recent patents on drug delivery & formulation* 2018: 12(3): 154-161.
- [54] Parasuraman, P., Antony, A. P., Sharan, A., Siddhardha, B., Kasinathan, K., Bahkali, N. A., ... & Syed, A. Antimicrobial photodynamic activity of toluidine blue encapsulated in mesoporous silica nanoparticles against *Pseudomonas aeruginosa* and *Staphylococcus aureus*. *Biofouling* 2019: 35(1): 89-103.
- [55] Sun, J., Fan, Y., Zhang, P., Zhang, X., Zhou, Q., Zhao, J., & Ren, L. Self-enriched mesoporous silica nanoparticle composite membrane with remarkable

- photodynamic antimicrobial performances. *Journal of colloid and interface science* 2020: 559: 197-205.
- [56] Mirzahosseini-pour, M., Khorsandi, K., Hosseinzadeh, R., Ghazaeian, M., & Shahidi, F. K. Antimicrobial photodynamic and wound healing activity of curcumin encapsulated in silica nanoparticles. *Photodiagnosis and photodynamic therapy* 2020: 29: 101639.
- [57] Paramanantham, P., Antony, A. P., Lal, S. S., Sharan, A., Syed, A., Ahmed, M., ... & Kaviyarasu, K. Antimicrobial photodynamic inactivation of fungal biofilm using amino functionalized mesoporous silica-rose bengal nanoconjugate against *Candida albicans*. *Scientific African* 2018: 1: e00007.
- [58] Bayir, S., Barras, A., Boukherroub, R., Szunerits, S., Raehm, L., Richeter, S., & Durand, J. O. Mesoporous silica nanoparticles in recent photodynamic therapy applications. *Photochemical & Photobiological Sciences* 2018: 17(11): 1651-1674.
- [59] Kuang, G., Zhang, Q., He, S., & Liu, Y. Curcumin-loaded PEGylated mesoporous silica nanoparticles for effective photodynamic therapy. *RSC Advances* 2020: 10(41): 24624-24630.
- [60] Park, S., Park, H., Jeong, S., Yi, B. G., Park, K., & Key, J. Hyaluronic acid-conjugated mesoporous silica nanoparticles loaded with dual anticancer agents for chemophotodynamic cancer therapy. *Journal of Nanomaterials* 2019.
- [61] Zhang, W., Shen, J., Su, H., Mu, G., Sun, J. H., Tan, C. P., ... & Mao, Z. W. Co-delivery of cisplatin prodrug and chlorin e6 by mesoporous silica nanoparticles for chemo-photodynamic combination therapy to combat drug resistance. *ACS applied materials & interfaces* 2016: 8(21): 13332-13340.
- [62] Han, R., Tang, K., Hou, Y., Yu, J., Wang, C., & Wang, Y. Fabrication of core/shell/shell structure nanoparticle with anticancer drug and dual-photosensitizer co-loading for synergistic chemotherapy and photodynamic therapy. *Microporous and Mesoporous Materials* 2020: 297: 110049.

- [63] Han, R., Tang, K., Hou, Y., Yu, J., Wang, C., & Wang, Y. Fabrication of core/shell/shell structure nanoparticle with anticancer drug and dual-photosensitizer co-loading for synergistic chemotherapy and photodynamic therapy. *Microporous and Mesoporous Materials* 2020 297: 110049.
- [64] Liu, Y., Liu, X., Xiao, Y., Chen, F., & Xiao, F. A multifunctional nanoplatform based on mesoporous silica nanoparticles for imaging-guided chemo/photodynamic synergetic therapy. *RSC advances* 2017 7(49): 31133-31141.
- [65] Kamkaew, A., Cheng, L., Goel, S., Valdovinos, H. F., Barnhart, T. E., Liu, Z., & Cai, W. Cerenkov radiation induced photodynamic therapy using chlorin e6-loaded hollow mesoporous silica nanoparticles. *ACS applied materials & interfaces* 2016: 8(40): 26630-26637
- [66] World Cancer Research Fund International. *Cancer Statistics*. (2020)
- [67] Swami, U., McFarland, T. R., Nussenzeig, R., & Agarwal, N. *Advanced Prostate Cancer: Treatment Advances and Future Directions*. *Trends in Cancer* 2020.
- [68] Litwin, M. S., & Tan, H. J. The diagnosis and treatment of prostate cancer: a review. *Jama* 2017: 317(24): 2532-2542
- [69] Kelly JF, Snell ME, Berenbaum MC: Photodynamic destruction of human bladder carcinoma. *Br J Cancer* 1975: 31:237–244.
- [70] Muschter, R. Photodynamic therapy: a new approach to prostate cancer. *Current urology reports* 2003: 4(3): 221-228
- [71] Sjoberg, H. T., Philippou, Y. J., Magnussen, A. L., Tullis, I. D., Bridges, E., Chatrian, A., ... & Bryant, R. J. Tumor irradiation combined with vascular-targeted photodynamic therapy enhances anti-tumor effects in preclinical prostate cancer. *bioRxiv* 2020.
- [72] Shi, X., Zhang, H., Jin, W., Liu, W., Yin, H., Li, Y., & Dong, H. Metronomic photodynamic therapy with 5-aminolevulinic acid induces apoptosis and

autophagy in human SW837 colorectal cancer cells. *Journal of Photochemistry and Photobiology B: Biology* 2019: 198: 111586.

- [73] Lin, C. H., Kumar Kankala, R., Busa, P., & Lee, C. H. Hydrophobicity-tuned periodic mesoporous organo-silica nanoparticles for photodynamic therapy. *International journal of molecular sciences* 2020: 21(7): 2586.
- [74] Bouffard, E., Mauriello Jimenez, C., El Cheikh, K., Maynadier, M., Basile, I., Raehm, L., ... & Morère, A. Efficient Photodynamic Therapy of Prostate Cancer Cells through an Improved Targeting of the Cation-Independent Mannose 6-Phosphate Receptor. *International journal of molecular sciences* 2019: 20(11): 2809.
- [75] Fidanzi-Dugas, C., Liagre, B., Chemin, G., Perraud, A., Carrion, C., Couquet, C. Y., ... & Léger, D. Y. Analysis of the in vitro and in vivo effects of photodynamic therapy on prostate cancer by using new photosensitizers, protoporphyrin IX-polyamine derivatives. *Biochimica et Biophysica Acta (BBA)-General Subjects* 2017: 1861(7): 1676-1690.
- [76] Akter, S., Saito, S., Inai, M., Honda, N., Hazama, H., Nishikawa, T., ... & Awazu, K. Efficient photodynamic therapy against drug-resistant prostate cancer using replication-deficient virus particles and talaporfin sodium. *Lasers in medical science* 2020: 1-8.
- [77] Li, J., Shen, S., Kong, F., Jiang, T., Tang, C., & Yin, C. Effects of pore size on in vitro and in vivo anticancer efficacies of mesoporous silica nanoparticles. *RSC advances* 2018: 8(43): 24633-24640.
- [78] Nadrah, P., Porta, F., Planinšek, O., Kros, A., & Gaberšček, M. Poly (propylene imine) dendrimer caps on mesoporous silica nanoparticles for redox-responsive release: smaller is better. *Physical Chemistry Chemical Physics* 2013: 15(26): 10740-10748.
- [79] Le, W., Chen, B., Cui, Z., Liu, Z., & Shi, D. Detection of cancer cells based on glycolytic-regulated surface electrical charges. *Biophysics Reports* 2019 5(1): 10-18.

- [80] Ziembra B, Janaszewska A, Ciepluch K, Krotewicz M, Fogel WA, Appelhans D, et al. In vivo toxicity of poly(propyleneimine) dendrimers. *J Biomed Mater Res*. 2011;99A:261–8.
- [81] Ji, C., Yuan, A., Xu, L., Zhang, F., Zhang, S., Zhao, X., ... & Guo, H. (2019). Activatable photodynamic therapy for prostate cancer by NIR dye/photosensitizer loaded albumin nanoparticles. *Journal of biomedical nanotechnology* 2019: 15(2): 311-318.
- [82] Cheng, G., & Li, B. Nanoparticle-based photodynamic therapy: New trends in wound healing applications. *Materials Today Advances* 2020: 6: 100049.
- [83] Topaloglu, N., Bakay, E., Yünlü, M., & Onak, G. Induced Photo-Cytotoxicity on Prostate Cancer Cells with the Photodynamic Action of Toluidine Blue Ortho. *Photodiagnosis and Photodynamic Therapy* 2021: 102306.
- [84] Xiang, Q., Qiao, B., Luo, Y., Cao, J., Fan, K., Hu, X., ... & Wang, Z. Increased photodynamic therapy sensitization in tumors using a nitric oxide-based nanoplatfrom with ATP-production blocking capability. *Theranostics* 2021: 11(4): 1953.
- [85] Deng, Y., Jia, F., Chen, S., Shen, Z., Jin, Q., Fu, G., & Ji, J. Nitric oxide as an all-rounder for enhanced photodynamic therapy: Hypoxia relief, glutathione depletion and reactive nitrogen species generation. *Biomaterials* 2018: 187: 55-65.
- [86] Chen, W. R., Adams, R. L., Bartels, K. E., & Nordquist, R. E. Chromophore-enhanced in vivo tumor cell destruction using an 808-nm diode laser. *Cancer Letters* 1995: 94(2): 125-131.
- [87] Zhang, Z. J., Wang, K. P., Mo, J. G., Xiong, L., & Wen, Y. Photodynamic therapy regulates fate of cancer stem cells through reactive oxygen species. *World Journal of Stem Cells* 2020: 12(7): 562.
- [88] Xu, D. D., Leong, M. M. L., Wong, F. L., Lam, H. M., & Hoeven, R. Photodynamic therapy on prostate cancer cells involve mitochondria membrane proteins. *Photodiagnosis and Photodynamic Therapy* 2020: 31: 101933.

- [89] D'Este, F., Della Pietra, E., Pazmay, G. V. B., Xodo, L. E., & Rapozzi, V. Role of nitric oxide in the response to photooxidative stress in prostate cancer cells. *Biochemical Pharmacology* 2020; 182: 114205.

Curriculum Vitae

Name Surname : Emel Bakay

E-mail : emelbakay@hotmail.com

Education:

2013–2018 İzmir Kâtip Çelebi University, Dept. of Biomedical Eng.

2018–2021 İzmir Kâtip Çelebi University, Dept. of Biomedical Eng.

Work Experience:

2016 Summer Internship Bursa Acıbadem Hospital

2017 Summer Internship Boğaziçi University

Publications (if any):

1. Avşar, N. T., Çağan, M., Bakay, E., & KOLKIRAN, A. (2021). Comparison of the effect of ethanol and potassium iodide in antibacterial photodynamic therapy on gram negative pathogens. *The European Research Journal*, 7(4), 348-355.
2. Topaloglu, N., Bakay, E., Yünlü, M., & Onak, G. (2021). Induced Photo-Cytotoxicity on Prostate Cancer Cells with the Photodynamic Action of Toluidine Blue Ortho. *Photodiagnosis and Photodynamic Therapy*, 102306.
3. AVŞAR, N. T., Bakay, E., & KOLKIRAN, A. (2020) Photodynamic action of chlorin e6 against methicillin resistant staphylococcus aureus with the aid of ethanol. *Archives of Clinical and Experimental Medicine*, 5(3), 100-105.
4. Şen Karaman, D., Ercan, U. K., Bakay, E., Topaloğlu, N., & Rosenholm, J. M. (2020). Evolving Technologies and Strategies for Combating Antibacterial Resistance in the Advent of the Postantibiotic Era. *Advanced Functional Materials*, 1908783.

Republic of Turkey
İzmir Kâtip Çelebi University
Graduate School of Natural and Applied Sciences

Enhancing the Anticancer Activity of Photodynamic Therapy with Dual Photosensitizers Incorporated Nanoparticle Design

Department of Biomedical Engineering
Master's Thesis

Emel Bakay
ORCID 0000-0002-3042-810X

Thesis Advisor: Dr. Nermin Topalođlu Avşar

August 2021

